Chng, M. H. Y., Lim, M. Q., Rouers, A., Becht, E., Lee, B., MacAry, P. A., Lye, D. C., Leo, Y. S., Chen, J., Fink, K., Rivino, L., & Newell, E. W. (2019). Large-Scale HLA Tetramer Tracking of T Cells during Dengue Infection Reveals Broad Acute Activation and Differentiation into Two Memory Cell Fates. *Immunity*, *51*(6), 1119-1135.e5. https://doi.org/10.1016/j.immuni.2019.10.007

Large Scale Epitope Tetramer Tracking and Phenotyping of Dengue-specific T Cells Over the Course of Acute Dengue Infection by Mass Cytometry

Melissa Hui Yen Chng[1], Cheryl Lim[2], Angeline Rouers[1], Etienne Becht[1], Bernett Lee[1], Paul A. MacAry[3], David Chien Lye[4,5,6,7,8], Yee Sin Leo[4,5,6,7,8], Jinmiao Chen[1], Katja Fink[1], Laura Rivino[2,9]*, Evan William Newell[1,10,11]*

Affiliations:

[1]Singapore Immunology Network, Agency for Science, Technology and Research, Singapore 138648, Singapore;

[2]Emerging Infectious Diseases Programme, Duke-NUS Medical School, Singapore 169857, Singapore;

[3]Immunology Programme, Department of Microbiology and Immunology, Life Science Institute, National University of Singapore, Singapore 117456, Singapore;

[4]National Centre for Infectious Diseases, Singapore 308442, Singapore.

[5]Tan Tock Seng Hospital, Singapore 308433, Singapore

[6]Lee Kong Chian School of Medicine, Singapore 308232, Singapore

[7]Yong Loo Lin School of Medicine, Singapore 119228, Singapore

[8]Saw Swee Hock School of Public Health, Singapore 117549, Singapore

[9]School of Cellular and Molecular Medicine, University of Bristol, Bristol, BS8 1TD, UK

[10]Vaccine and Infectious Disease Division, Fred Hutchinson Cancer Research Center, Seattle Washington 98109, USA

[11]Lead Contact

*Correspondence and equal contribution: laura.rivino@bristol.ac.uk (L.R.) or enewell@fredhutch.org (E.W.N.)

SUMMARY

T cells play important roles in protection during dengue virus (DENV) infection and in the immunopathogenesis of dengue fever. Using mass cytometry and a highly-multiplexed peptide-HLA tetramer staining strategy, we probed T cells from dengue patients for a total of 430 dengue and control candidate epitopes presented on HLA A*1101, A*2402, and B*5801, together with key markers of activation, trafficking, and differentiation. We found that expression of PD-1, ICOS, CD39, CD69, and GPR56 on dengue-specific T cells varied significantly depending on HLA type. We also phenotypically profiled diverse T cell subsets and NK cells. Acute dengue infection resulted in broad activation and proliferation of these cells. During the acute stage, dengue-specific $CD8^+$ T cells expressed a unique profile of activation and trafficking receptors that distinguished them from non-dengue specific T cells. During convalescence dengue-specific T cells differentiated into two major cell fates, $CD57^+$ $CD127^-$ terminally differentiated senescent memory cells and $CD127^+$ $CD57^-$ proliferation-capable memory cells. The long-term maintenance of dengue-specific T cells with these phenotypes was evaluated in a second cohort of dengue patients and these subsets were found at elevated frequencies up to one year after infection. These analyses aid our understanding of the generation of T cell memory in dengue infection or vaccination.

Keywords: mass cytometry, cytof, dengue, T cell, memory, CD57, IL-7R, CD127, DENV, tetramer

INTRODUCTION

Dengue virus (DENV) is the most significant mosquito-borne flavivirus, estimated to cause up to 390 million infections per year, of which 100 million cases are symptomatic (Bhatt et al., 2013). Dengue fever is caused by infection of any of four infectious DENV serotypes (DENV 1 - 4) that are endemic to more than 100 countries worldwide (Messina et al., 2014). At present, there is no antiviral therapy, and the sole approved vaccine, CYD-TDV, has demonstrated protective efficacy only for vaccinees with a serostatus indicating history of prior infection with DENV, and is thus recommended for use only in these populations (Sridhar et al., 2018).

Symptomatic DENV infection typically results in a self-limiting febrile illness which coincides with viremia, lasts approximately 5 days, and is followed by recovery and the complete disappearance of DENV from the blood (Vaughn et al., 1997). Robust T cell activation is detected in the blood upon resolution of viremia and fever (Dung et al., 2010). Dengue infection can also manifest as more severe life-threatening dengue hemorrhagic fever (DHF) and dengue shock syndrome that are characterized by plasma leakage and hemorrhagic manifestations. Findings from epidemiological studies, as well as from clinical trials of the CYD-TDV vaccine, indicate that these forms of severe dengue are closely associated with secondary heterotypic DENV infection (Guzmán et al., 1990; Sridhar et al., 2018).

Original antigenic sin, as applied to dengue infection, is the theory that memory T and B cells that arise from primary infection by one serotype of DENV or unequal immunogenicity by a vaccine, when encountering secondary infection with a different serotype of DENV, mount a cross-reactive but suboptimal and immunopathogenic response against the new serotype (Mongkolsapaya et al., 2003). The current lack of success in developing a universal dengue

vaccine has underlined the importance of understanding the immune response to natural dengue infections, defining correlates of protective immunity to dengue, as well as finding effective vaccine antigens (Sridhar et al., 2018; St John and Rathore, 2019).

Dengue-specific $CD8^+$ T cells mainly target the DENV non-structural proteins NS3, NS4, and NS5 while $CD4^+$ T cells predominantly recognize epitopes from the structural proteins capsid/envelope and the secreted protein NS1 (Chandele et al., 2016; Duangchinda et al., 2010; Dung et al., 2010; Rivino et al., 2013; Simmons et al., 2005; Weiskopf et al., 2013, 2015). Despite the abundance of known T cell epitopes for dengue, single-cell studies using peptide-HLA tetramers and flow cytometry have focused on the analysis of T cells targeting a few well characterized epitopes (Friberg et al., 2011; Mongkolsapaya et al., 2003, 2006; Rivino et al., 2015; Simmons et al., 2005; Townsley et al., 2014). Alternatively, studies analyzing T cell responses targeting a broad range of epitopes have utilized peptide pools to stimulate bulk T cells, thus sacrificing in-depth epitope-specific single cell data (Tian et al., 2019; Weiskopf et al., 2013, 2015). However, dengue-specific memory T cells from individuals restricted to different HLA molecules differ significantly in terms of magnitude, phenotype and ability to produce cytokines (Weiskopf et al., 2013), indicating that there is much to be learned from studying T cell responses to a broad range of dengue epitopes at single cell resolution.

To overcome these challenges in capturing both the depth and the breadth of the T cell response to natural dengue infection, we used mass cytometry to probe single cells with 44 parameters at a time. In conjunction with highly multiplexed combinatorial peptide-HLA tetramer staining (Newell et al., 2013), we were able to screen for a total of 430 dengue and control candidate antigens in patients who expressed HLA-B*5801, HLA-A*1101, and HLA-A*2042, while

simultaneously measuring 27 activation and trafficking markers on $CD8^+$ T cells. To understand the interplay between $CD8^+$ T cells and the wider immune context, we also used a second complementary panel of markers for diverse T cell subsets and NK cells and performed Luminex analysis for cytokines in longitudinal plasma samples. Lastly, we were able to validate and extend some of our findings in a separate, larger patient cohort, which also included an analysis of dengue-specific T cells that were detectable one year after infection.

Our data from *ex vivo* human peripheral blood samples shows that dengue infection resulted in broad activation and proliferation of multiple different immune cells at the acute stage of disease, but most of these biomarkers rapidly returned to baseline levels by the post-febrile stage. With tetramer screening, we were able to detect T cells specific for 21 unique antigen-HLA combinations, which allowed us to analyze the impact of epitope immunodominance and HLA type on dengue-specific T cell phenotypes. Lastly, through trajectory analysis of dengue-specific T cell differentiation, we identified that dengue-specific T cells differentiated into two major populations: $CD57^+$ $CD127^-$ cells that phenotypically resemble descriptions of terminally differentiated senescent memory cells and $CD127^+$ $CD57^-$ cells that resemble proliferation-capable memory cells. We observed that these populations were stably maintained up to one year post infection.

RESULTS

Acute Dengue Infection Causes Broad Activation of Various Immune Cells

To understand how dengue infection affects various immune populations, we obtained dengue patient PBMCs during the following stages of dengue infection: acute (5-9 days post fever onset), post-febrile (14-28 days) and early convalescent (45-78 days). Clinical details for the first cohort are catalogued in Table S1A and comparisons between the main study cohort (Mab) and the second validation cohort (LNA, described later) are summarized in Table S1B. Mab cohort cells were stained with an antibody panel which focused on markers for T cell subsets, but also included markers for B cells and NK cells (Table S2), and were then acquired using a mass cytometer. We performed UMAP analysis (Becht et al., 2018a; McInnes and Healy, 2018) on live $CD45^+$ $CD14^-$ cells and identified 9 separate clusters (Fig 1A, B): $CD4^+$ T cells, $CD8^+$ T cells, $V\delta1^+$ $\gamma\delta$ T cells, $V\delta2^+$ $\gamma\delta$ T cells, MAIT cells, B cells, $CXCR5^-$ B cells, plasmablasts, and NK cells.

Comparisons of UMAP plots from acute, post-febrile and early convalescent time points indicated that significant increases in cells expressing Ki67, a marker of cell proliferation, occurred at the acute time point and that these cells diminished with time (Fig 1C). Using a manual gating strategy (Fig S1A), we found that while only frequencies of plasmablasts and $CXCR5^-$ B cells showed significant increases during acute infection (Fig S1B, Table S3), when we quantified the frequency of $Ki67^+$ cells in each immune subset, all of the immune cell subsets except for B cells showed large expansions of $Ki67^+$ cells at the acute stage (Fig 1D), indicating that dengue infection was causing proliferation of these immune cell subsets.

With such simultaneous activation of multiple different immune cells, we hypothesized

that plasma cytokines might be helping to coordinate this effect. We used Luminex to measure 75 plasma cytokines (Table S4). Using principle component analysis (PCA), we found that acute samples clustered separately from post-febrile and early convalescent samples, which clustered together (Fig S1C). A broad range of cytokines showed significant increases at just the acute time point (Fig 1E), including pro-inflammatory cytokines, IFN-γ, IFN-γ-promoted chemokines, and biomarkers of tissue damage. CCL24 (Eotaxin-2), a chemokine for eosinophils, was the only cytokine that increased with recovery time. Interestingly, one study found that peripheral blood eosinophils progressively increased from acute to convalescent stages of dengue (Wells et al., 1980).

In-Depth Analysis of Immune Cell Subsets Shows the Same Pattern of Acute Stage Activation

UMAP and Louvain clustering analyses using Phenograph (Levine et al., 2015) were performed on $CD4^+$ (Fig 2A) and non-MAIT $CD8^+$ T cells (Fig 3A). Clusters identified by Phenograph were then named by comparing the median expression of relevant markers (Fig 2B, 3B) to immune cell subsets reported in the literature (Acosta-Rodriguez et al., 2007; Gosselin et al., 2010; Kunicki et al., 2017; Weiskopf et al., 2015; Wong et al., 2015). Jensen Shannon Divergence indices between these subsets were calculated to quantify the differences between each subset (Fig S2A). Hypergate was used to identify the optimum gating strategies for these clusters (Fig S2B-E) (Becht et al., 2018b), which were used for subsequent enumeration of cellular frequencies across batches.

While overall frequencies of $CD4^+$ T cell subsets did not appear to change significantly

over time, except for Th2 cells, which trended upward with recovery time (Fig 2C), frequencies of Ki67$^+$ cells were significantly increased during acute infection in the central memory (CM), effector memory (EM), effector memory RA (EMRA) (Sallusto et al., 1999), Th1-like follicular helper cells (Th1-like TFH), Th1, CD57$^-$ Cytotoxic CD4$^+$ T, Th1Th17, and Treg subsets (Fig 2D).

We also analyzed CD4$^+$ T cells for markers or marker combinations associated with activation and trafficking (Fig 2E, Fig S2F). For example, CD38$^+$ CCR7$^-$ CD4$^+$ T cells have been shown to be expanded and enriched for antigen-specific CD4$^+$ T in the context of salmonella infection (Napolitani et al., 2018). As expected, we observed increased frequencies of CD38$^+$ CCR7$^-$, CD69$^+$ and ICOS$^+$ PD-1$^+$ CD4$^+$ T cells. In addition, CCR4$^+$ cells increased with recovery. CCR4 and Ki67 expression tended to be mutually exclusive (Fig S2G), so this increase is probably due to the gradual decrease of Ki67$^+$ CCR4$^-$ cells.

In CD4$^+$ T cells, Th1 and Treg cells were the only subsets to have separate clusters of Ki67$^-$ and Ki67$^+$ cells identified by Phenograph (Fig 2B). We observed that compared to Ki67$^-$ Th1 cells, Ki67$^+$ Th1 cells had higher expression of CD38, ICOS, Granzyme B, PD-1, TBET, CCR5, HLA-DR, and CD69. Many of these markers have been observed on CCR5$^+$ CD38^{hi} antigen-specific Th1 effector cells that proliferate in the early stages of primary HIV-1 infection (Zaunders et al., 2005). In quantifying the changes of these markers with time, we found that the frequencies of CD38$^+$ CCR7$^-$, CD69$^+$, ICOS$^+$ PD-1$^+$, CCR5$^+$, and TBET$^+$ Th1 cells mirrored the dynamics for Ki67 expression in Th1 cells (Fig 2F).

Treg cells have previously been shown to increase Ki67 expression during acute dengue (Jayaratne et al., 2018; Lühn et al., 2007). Fig 2B indicated higher median expression of trafficking markers such as CCR4, CCR5 or CLA in Ki67$^+$ Treg cells relative to Ki67$^-$ Treg cells. Again, CD38$^+$

CCR7^{-}, CD69^{+}, and ICOS^{+} PD-1^{+} Treg frequencies were increased only during acute disease (Fig 2F). Interestingly, CCR4^{+} Treg cells increased over time. CD4^{+} CCR4^{+} cells were CD45RO^{+} and FOXP3-enriched (Fig S2H), which have previously been identified as effector Treg, a more suppressive Treg subset compared to naïve Treg cells (Sugiyama et al., 2013).

Ten clusters were identified in CD8^{+} T cells (Fig 3A, B). Clusters 5 to 10 were Granzyme B^{+} effector T cells that were distinguished by combinations of positive or negative Helios, CD57, and Ki67 expression. Overall frequencies of the different CD8^{+} subsets did not change significantly (Fig 3C) but all subsets showed significant increases of Ki67^{+} cells during acute dengue only (Fig 3D). This pattern was mirrored by frequencies of HLA-DR^{+} CD38^{+}, CD69^{+}, and ICOS^{+} PD-1^{+}, as well as cutaneous lymphocyte antigen (CLA)- expressing CD8^{+} T cells (Fig 3E). CLA is a skin homing receptor which has been shown to be upregulated on dengue-specific CD4^{+} and CD8^{+} T cells, as well as NK cells in response to dengue infection (Keawvichit et al., 2018; Rivino et al., 2015). Lastly, frequencies of CD103^{+} T cells and CCR4^{+} EM cells trended upward with recovery time (Fig 3E, F).

Similar patterns of increased expression of Ki67, CD38 or CD69 at the acute stage only were observed for MAIT cells, Vδ1^{+} and Vδ2^{+} $\gamma\delta$ T cells, NK cells, NK cell subsets, and B cells (Fig 3G-K).

To analyze heterogeneity between individuals, we performed PCA on the frequencies of these broad subsets (Table S3, Fig S3A). The different timepoints spread out along the PC1 axis, which unsurprisingly was dictated by the frequencies of Ki67^{+} subsets (Fig S3B). Along the PC2 axis, interindividual heterogeneity appeared to receive the strongest contributions from the frequencies of TBET^{+} and naïve CD8 T cells (Fig S3C).

Peptide-HLA tetramer screening enables epitope-specific analysis of T cell responses.

Using highly multiplexed peptide-HLA tetramers, we screened for a total of 430 dengue and control antigens (Table S2) while measuring 27 activation and trafficking markers on T cells. An example of tetramer$^+$ staining is shown in Fig 4A. Across 16 patients and 3 healthy controls, we detected 9 different dengue epitopes presented by HLA-B*5801, 7 presented by HLA-A*1101, and 5 presented by HLA-A*2402, as well as Epstein-Barr Virus (EBV), flu, and human cytomegalovirus (CMV) control epitopes (Table S5). Since the CMV epitopes were detected in only one patient and at low frequencies, they were left out of subsequent analysis. We also found two epitopes in the M region of dengue that had not been previously reported in the literature before (Fig S4A). For further patient-specific detail, the frequencies of epitope-specific T cells, IFN-γ ELISPOT results from stimulation with pools of the same epitopes used for tetramer screening, and the diversity of hits within each patient are included in Fig S5A. We also computed the JSD values for distances between individual samples on the UMAP plot in Fig 4E and found that distances were dictated by time points, rather than individuals (Fig S5B). The number of epitopes detected for each patient varied significantly. Between zero and nine of the epitopes used in the tetramer screen were detected in each patient (Fig S5C). Our ELISPOT results for individual patients, as well as total ELISPOT results, largely mirrored the detected frequencies of dengue tetramer$^+$ T cells (Fig S5A, D).

Data for frequencies of dengue epitope-specific CD8$^+$ T cells are summarized in Fig 4B. HLA-B*5801 epitopes $NS5_{3174\text{-}3182}$ (magenta) and $NS5_{3287\text{-}3295}$ (red) as well as HLA-A*1101 epitope $NS3_{1608\text{-}1617}$ (blue) were labelled as dominant epitopes because they were detected in multiple patients and in some of these patients, they were the most frequent epitope detected (Fig 4D,

S5A). HLA-A*2402 epitope $NS5_{2974-2983}$ (brown) was detected in only one patient but at the highest frequencies in the whole study. We could not determine any upward or downward trend in the frequencies of these cells over time. When the frequencies of individual epitopes were summed up into the total frequencies for each patient, early convalescent frequencies correlated strongly with post-febrile but not acute frequencies (Fig 4C). This is in line with previous observations made in recipients of the live attenuated vaccine to the yellow fever virus (YFV), which is in the same genus as DENV (Akondy et al., 2015). The number of patients from which each epitope was detected is summarized in Fig 4D. As has previously been shown, the epitopes detected were most commonly derived from the NS3 and NS5 antigens (Duangchinda et al., 2010; Rivino et al., 2013).

Using UMAP analysis, we determined that unlike the tetramer-negative $CD8^+$ T cells, the vast majority of dengue, EBV and flu $tetramer^+$ T cells were not naïve cells (Fig S4B). This non-random skewing of the phenotypes of these $tetramer^+$ T cells fits with the expected biology and helped to confirm that the tetramer staining and curation process were reliable. During acute dengue infection, dengue-specific T cells expressed Ki67 and many other activation markers which positioned these cells in their own section of the UMAP plot, whereas dengue-specific T cells collected at the post-febrile and early convalescent stages were more quiescent and similar to each other (Fig 4E, S4C). For these patients, we did not observe EBV and flu $tetramer^+$ T cells experiencing bystander activation during natural dengue infection, in line with prior reports in dengue infection and YFV vaccine studies (Friberg et al., 2011; Miller et al., 2008), and these cells were sufficiently different from dengue-specific T cells and each other to occupy their own regions of the UMAP plot.

One hypothesis that has been put forward is that HLA type affects immunogenicity and consequently, T cell responses to the epitopes presented, leading to protection or susceptibility to dengue infection (Paul et al., 2013; Weiskopf et al., 2013). While we did not observe differences in the overall UMAP distributions of T cells recognizing epitopes derived from the same virus but presented by different HLA molecules (Fig. S4D), when we analyzed early convalescent dengue-specific T cells further, we observed that T cells that bound HLA-A*1101 tetramer expressed less PD-1 compared to T cells that bound to HLA-A*5801 tetramer (Fig 4F, G). We quantified the PD-1$^+$ populations in these cells according to each unique antigen and found that HLA-B*5801 tetramer$^+$ T cells had significantly more PD-1$^+$ cells than HLA-A*1101 and A*2402 tetramer$^+$ T cells (Fig 4H). This result is strikingly similar to the results in which HLA-B*3501 dengue tetramer$^+$ T cells expressed more PD-1 than HLA-A*2402 dengue tetramer$^+$ T cells (de Alwis et al., 2016).

We also hypothesized that epitope dominance might affect T cell responses. We compared the UMAP distributions of T cells specific for dominant HLA-B*5801 epitopes, $NS5_{3174-3182}$ and $NS5_{3287-3295}$, as well as HLA-A*1101 epitope, $NS3_{1608-1617}$, against all the other subdominant epitopes but found no obvious differences (Fig S4E). Frequencies of PD-1$^+$ cells were also not significantly different between dominant and subdominant epitopes (Fig 4H).

Peptide-HLA tetramer screening enables disease-specific analysis of T cell responses.

Pooled dengue, EBV, and flu tetramer$^+$ cells as well as Naïve, CM, EM, EMRA, and Ki67$^+$ populations in tetramer-negative CD8$^+$ T cells were analyzed for positive expression of activation

and trafficking markers, and the mean frequencies were summarized in a heatmap (Fig 5A). During acute infection, dengue-specific T cells expressed a unique combination of activation and trafficking markers that EBV- and flu-specific T cells did not, such as CD38, HLA-DR, Ki67, ICOS, Granzyme B, and CLA, mirroring observations in experiments using the YFV vaccine (Miller et al., 2008). Also CLA has been shown to be preferentially expressed in dengue-specific T cells but not CMV-specific T cells during acute dengue (Rivino et al., 2015). Acute stage dengue-specific T cells matched most closely to bulk $Ki67^+$ $CD8^+$ T cells in expression signature, but early convalescent stage dengue-specific T cells did not map neatly to the standard naïve, CM, EM, and EMRA categories. The combination of CD57 and Granzyme B expression looked like promising markers for identifying dengue-specific T cells at the early convalescent stage. However, about 10% of $CD8^+$ T cells in healthy controls were also $CD57^+$ Granzyme B^+ (Fig S4F). Hence, at the post-febrile and early convalescent stages, peptide-HLA tetramers were crucial for separating dengue-specific T cells from bystander T cells.

Further analysis of dengue-specific T cells over time confirmed that most activation and trafficking markers were expressed early and declined except for CD57 and CD45RA which increased with time (Fig 5B). We also compared dengue-specific T cells with EBV and flu-specific T cells from early convalescent stage samples (Fig 5C). Compared to EBV and flu, dengue-specific T cells tended to be negative for CD103, CXCR3, CCR5, CD95, and CD127 but were enriched for CD57 and Granzyme B expression. Meanwhile, EBV-specific T cells had lower CD161 and CD49d expression but higher Integrinβ7 expression than dengue or flu-specific T cells. Lastly, flu-specific T cells had weaker expression of HLA-DR and CD27 but higher expression of CXCR6 and CLA compared to EBV and dengue.

Trajectory Analysis of Dengue-specific T cells Reveals Two Differentiation Trajectories

Monocle-2 is a robust and popular trajectory inference method that can predict any number of branches and requires no prior knowledge, which makes it a useful tool for unsupervised trajectory analysis (Qiu et al., 2017). With our data set, Monocle-2 correctly ordered cells from the different time points without our input and predicted one branch point arising around the transition from post-febrile to early convalescent stage and two cell fates (Fig 6A). The heatmap in Figure 6B shows the expression of all the markers along the branches, going from the pre-branch stage to Cell Fate 1 or Cell Fate 2. The branch to Cell Fate 1 was characterized by increasing expression of CD57, CD161, Granzyme B, and CD45RA while the branch to Cell Fate 2 was characterized by increasing CD127, CCR7, CD103, CXCR3, and CD45RA expression. CD57 and CD127 are the markers that most uniquely define each cell fate (Fig 6C).

CD127 marks memory or memory precursor T cells that can proliferate and give rise to long-lived memory cells (Cellerai et al., 2010; Kaech et al., 2003), while $CD57^+$ $CD8^+$ T cells are senescent and cytotoxic effector or effector memory T cells that contain Granzyme B (Brenchley et al., 2003; Chattopadhyay et al., 2009). When dengue-specific T cells were analyzed for CD57 and CD127 expression, the acute stage had negligible frequencies of cells with positive expression for these markers, in keeping with these markers only being expressed after early activation (Fig 6D, E). At the post-febrile and early convalescent stages, the frequencies of $CD57^+$ and $CD127^+$ dengue-specific cells both increased but with considerable skewing toward the $CD57^+$ cells. In comparison, EBV and Flu-specific T cells were composed of higher frequencies of $CD57^-$ $CD127^+$ cells and $CD57^+$ $CD127^+$ cells and fewer single positive $CD57^+$ cells (Fig 6D).

We examined how the $CD57^+$ $CD127^-$ and $CD127^+$ $CD57^-$ cell fates related to standard

memory subset categories. Most of the $CD57^+$ $CD127^-$ cells were terminally differentiated EM and EMRA cells (Fig 6F). On the other hand $CD127^+$ $CD57^-$ cells contained a significant population of $CCR7^+$ $CD45RA^+$ $CD45RO^-$ cells, which also expressed CXCR3 and CD95 (Fig 6B) and closely resemble stem cell-like memory cells (Gattinoni et al., 2011).

We hypothesized that the intensity of immune activation during the acute stage of dengue might affect the composition of the immune system at the early convalescent stage. To investigate this, we performed large scale analyses of associations between acute and early convalescent on all the measurements that had thus far been shown to be significantly increased or decreased over the course of dengue infection since these were likely to be dengue-relevant (Figure S6, Table S6). Most significant correlations were between nodes from the same time point and the network was dominated by related subsets, probably reflecting the overabundance of redundant activation markers that were selected for by our previous analysis and assumptions.

Validation of Findings in Separate Dengue Cohort

Some concerns about the first cohort were the relatively small number of patients and the early endpoint of the study which might prevent us from observing the true endpoint of T cell differentiation. Subsequently, we also analyzed a second larger dengue patient cohort that was followed until one year after acute dengue infection, LNA. While a separate manuscript for the key findings for the LNA study, which are distinct from the ones here, is in preparation, there was significant overlap in the two study methodologies that we were able to validate some of our findings in the second patient cohort. For the LNA cohort, Singapore adult patients were recruited

at the same study site as the Mab cohort with PBMCs obtained at 4 time points: acute, post-febrile, late convalescent, and late (Table S1B).

In addition to confirming that the HLA-B*5801-specific increase for PD-1 shown in Fig 4H persists in late convalescent dengue-specific T cells (Fig 7A), we also observed that HLA-A*2402 dengue-specific T cells had relatively depressed frequencies of $ICOS^+$ cells. In the LNA cohort, we also found that at the acute stage, CD39 expression was lower in T cells that bound HLA-A*1101 dengue tetramers, CD69 was lower in HLA-A*2402-specific T cells, and GPR56 was highest in HLA-A*5801-specific T cells (Fig 7B).

Interestingly, Monocle-2 predicted three cell fates for the dengue-specific T cells in our second cohort, as can be seen in terminal branches 2, 4, and 5 (Fig 7C). The two major cell fates 2 and 4, were similar to the two cell fates in the first cohort as they were defined by CD57 and CD127 expression respectively, while expression of markers in the new cell fate, 5, lay between the two extremes (Fig 7D, E). As in the Mab cohort, the $CD57^+$ $CD127^-$ population in this cohort was also enriched for CD161 and Granzyme B. In addition, they also upregulated expression of CX3CR1, CD16, KLRG1, GPR56. This constellation of markers fits with an effector T cell program that is cytotoxic and senescent (Bengsch et al., 2018; Ibegbu et al., 2005) and the upregulation of CD45RA and persistence of this population one year after infection suggests that these cells have become memory cells (Akondy et al., 2009). The $CD127^+$ $CD57^-$ population also recapitulated the upregulation of CCR7, CXCR3, and CD45RA seen in our earlier findings.

In the second cohort, we observed that in the late convalescent and late stages, the $CD127^+$ $CD57^-$ population reached higher frequencies than the $CD57^+$ $CD127^-$ population (Fig 7F). The differences in the findings for the two cohorts might be explained by the late convalescent

timepoint being more than two times later than the early convalescent timepoint, such that sufficient time has passed for the $CD127^{+}$ $CD57^{-}$ memory cells to proliferate to greater numbers than the $CD57^{+}$ $CD127^{-}$ effector cells.

DISCUSSION

This work is, to our knowledge, the most extensive effort to date to directly characterize the impact of natural dengue infection on human T cell activation and differentiation. We tracked $CD8^+$ T cells with various ligands, alongside the immune milieu made up of $CD4^+$ T cells, unconventional T cells, NK cells, B cells, plasmablasts, and cytokines, and related them all together. A pattern that quickly emerged was that dengue infection caused broad activation and proliferation of innate as well as adaptive immune cells during acute disease. As the patients recovered, we observed a rapid return of immune cell activation and proliferation markers to baseline, such that the post-febrile and early convalescent stages showed similar patterns of activation. Since the acute time point was consistently the time point at which biomarkers were found to significantly diverge from the other two time points, we chose to focus most of our analyses on changes specific to this time point since we could be certain these changes were dengue-relevant.

Th1 and Th1-like cells, such as Th1-like TFH and Th1Th17 cells (Acosta-Rodriguez et al., 2007; Weiskopf et al., 2015), appeared to be preferentially activated in dengue infection. They were also all CXCR3-expressing. Another activated subset, $CD57^-$ Cytotoxic $CD4^+$ T cells, expressed moderate levels of CXCR3. CXCR3 binds to CXCL4, CXCL9 (MIG), CXCL10 (IP-10), and CXCL11 (I-TAC) (Bachelerie et al., 2014). Of these chemokines, MIG, IP-10, I-TAC and MDC were included in our Luminex experiment. MIG, IP-10, and I-TAC were all significantly elevated during acute dengue in our study, as well as in others (Conroy et al., 2015; Her et al., 2017; Huang et al., 2018; Rathakrishnan et al., 2012). These cytokines could explain the presence and/or activation of $CXCR3^+$ subsets in peripheral blood. CXCR3 and IP-10 are important for $CD4^+$ and $CD8^+$ T cell

trafficking to the brain in murine intracerebral dengue infection (Hsieh et al., 2006), while in human patients, higher IP-10 levels correlated with severe disease like DHF (Conroy et al., 2015) or severe plasma leakage (Her et al., 2017).

In accordance with other studies, we observed significant activation and proliferation of unconventional T cells, like MAIT cells (Paquin-Proulx et al., 2018; van Wilgenburg et al., 2016), γδ T cells (Green et al., 1999; Tsai et al., 2015), B cell-derived plasmablasts (Wrammert et al., 2012), and innate immune cells, like NK cells (Green et al., 1999; Keawvichit et al., 2018; Petitdemange et al., 2016) during acute dengue. MAIT and γδ T cells have restricted ligand repertoires compared to αβ T cells and sense viruses via TCR-independent mechanisms. For example, MAIT cells use a semi-invariant TCR (Vα7.2-Ja12/20/33) that is restricted by the highly evolutionarily conserved, MHC class Ib molecule, MR1 (Treiner et al., 2003). Antibody blocking of MR1 did not inhibit activation of MAIT cells in co-culture exposed to DENV (van Wilgenburg et al., 2016). Instead virally triggered IL-18 correlated with MAIT cell activation in dengue-infected patient samples and antibody blocking of IL-18 in *in vitro* co-cultures with DENV inhibited MAIT activation. Similarly, γδ T cells express invariant γδ TCRs, which recognize various non-standard antigens, like MHC class I chain-related antigens A and B, phosphoantigens or lipids (Vermijlen et al., 2018). Again, IL-18 is important for activation of γδ T cells to produce IFN-γ (Tsai et al., 2015). In our study, IL-18 was one of the cytokines that significantly increased in acute dengue. IL-18, together with IL-12, promotes IFN-γ production in a TCR-independent fashion (Yang et al., 2001). NK, MAIT, $CD8^+$ T, Th1, Th1-like TFH, Th1Th17, and cytotoxic $CD4^+$ T cells are all producers of IFN-γ (Gosselin et al., 2010; Paquin-Proulx et al., 2018; Weiskopf et al., 2013, 2015; Wong et al., 2015), and their activation mirrors the acute stage increase of IFN-γ recorded in our study. Given that

the CXCR3-binding cytokines, MIG, IP-10, and I-TAC are all primarily regulated by IFN-γ (Metzemaekers et al., 2018), this could set up a positive feedback loop that leads to cytokine storms and more severe forms of dengue.

Several studies have sought to establish associations between HLA presentation to dengue-specific T cells and clinical protection from or susceptibility to dengue infection. (Weiskopf et al., 2013) performed IFN-γ ELISPOT experiments on HLA-restricted T cell responses to dengue epitopes across a gamut of HLA-A and HLA-B types. Overall, they argued that HLA-B-restricted responses reached higher magnitudes than HLA-A-restricted responses. In particular, their data set showed that T cell responses to HLA-B*5801-presented epitopes reached a higher magnitude than T cell responses to HLA-A*1101 and A*2402. In our study, HLA-B*5801 tetramer$^+$ T cells showed higher expression of activation markers ICOS, PD-1, CD69, as well as CD39 and GPR56, compared to the other two HLA types. CD39 is believed to be a marker of exhausted CD8 T cells, especially tumor-specific CD8$^+$ T cells, (Simoni et al., 2018), although in this study of acute infection, we only observed its upregulation at the acute timepoint. GPR56 marks CD4$^+$ TEMRA cells that are viral epitope specific (Tian et al., 2017). As such, our findings may support the hypothesis that HLA-B*5801 presentation of dengue epitopes might be more efficient at activating T cells than HLA-A*1101 and A*2402. However, we would like to caution that our data doesn't explain how this might translate to protection from disease or clinical outcome in dengue. Similarly, the study by (Weiskopf et al., 2013) did not discuss the clinical outcomes of dengue infection in their donors, making it difficult to draw conclusions on how HLA types affect these.

During acute infection, the dengue-specific CD8$^+$ T cells in our patient groups were

relatively homogeneous in their upregulation of activation markers and trafficking receptors, such as Ki67, HLA-DR, and CD38, but during the post-febrile and later stages, these cells differentiated along two main paths, such that from 45 days to one year after fever onset we could distinguish two distinct subsets of dengue-specific T cells ("cell fate 1" and "cell fate 2"). Two markers, CD57 and CD127, most uniquely define cell fate 1 and 2, respectively. CD57 is a marker of T cell differentiation and senescence, the expression of which correlates with increased cytolytic ability but reduced proliferative and survival capacity in human memory $CD8^+$ T cells (Priol et al., 2006). CD127, the IL-7Rα chain, is expressed early after T cell activation and in mice marks virus-specific T cells that survive to become long-term memory cells, i.e. display proliferative and recall capacity, as well as ability to survive in the absence of antigen (Kaech et al., 2003). Similarly, virus-specific $CD127^+$ memory cells in humans proliferate vigorously following peptide stimulation or in response to IL-7 and/or IL-15, whereas their $CD127^-$ counterparts require both peptide and $CD4^+$ T cell help, IL-2 or IL-15 for optimal expansion (van Leeuwen et al., 2005). In addition to CD57, cells that belong to cell fate 1 upregulated a constellation of markers that have been described for cytotoxic effector T cells: granzyme B, CX3CR1, CD16, KLRG1, and GPR56 (Bengsch et al., 2018; Chattopadhyay et al., 2009). The cells from cell fate 2 upregulated memory-like features: CD127, CCR7, CD103, and CXCR3 (Akondy et al., 2017; Gebhardt et al., 2009; Sallusto et al., 1999). Lastly, both cell fates upregulated CD45RA, which has been considered a sign of T cell memory formation in studies using the live attenuated YFV vaccine (Akondy et al., 2009; Blom et al., 2013).

Identifying our $CD57^+$ $CD127^-$ cell subset posed a conundrum because of different theories on what constitutes an effector, EM, or EMRA cell and the order of differentiation for these cells.

By the widely used definitions laid out by (Sallusto et al., 1999) , these cells bear the features of effector cells and EMRA cells, and EMRA cells are considered to be terminally differentiated. In a series of papers on T cell responses to the YFV vaccine, YF-17D, Rafi Ahmed et al. laid out an alternative timeline of single pathway differentiation of effector T cells into memory T cells. First, they found that all of their YF-17D tetramer^{+} T cells expressed perforin and granzyme B, which are mediators of effector CD8^{+} T cell killing, at the peak of the response to the vaccine (day 14) and suggested that this meant that this was an obligate phase that vaccine-responsive T cells must pass through before differentiating into memory T cells (Miller et al., 2008). These cells were also characterized as being HLA-DR^{+}, CD38^{+}, Ki67^{+}, and BCL-2^{lo}. Subsequently, they showed that YF-17D-specific cells were nearly 100% positive for Ki67^{+} and about 80% positive HLA-DR+ CD38+ subsets at the same time point post immunization (Akondy et al., 2009). The frequency of cells positive for these markers decreased with time, while the percentage of CD127+ cells decreased and then increased at day 90, at the point that they considered these cells to be memory cells. Our study recapitulates many of these results for dengue infection, but we see a substantial CD57+ population in our convalescent and late stage dengue tetramer^{+} T cells, while they did not in their YF-17D tetramer^{+} cells. However, they noted bimodal expression patterns of granzyme B in their memory T cell populations (Miller et al., 2008), and our dengue-specific T cells bifurcate into CD57^{+} granzyme B^{+} and CD127^{+} granzyme B^{-} cells. Finally, in an elegant study, they tracked YFV vaccine-specific CD8^{+} T cells with deuterium labelling out to 750 days *in vivo*, revealing that at least a fraction of the cells present at the point of vaccination became long-lived memory CD8^{+} T cells that retained epigenetic marks associated with a history of having been an effector cell (Akondy et al., 2017). Effector and memory T cells were defined by the time point

after vaccination (effector; days 14-28, memory; day 90 or later, long term memory; 3 or more years later), not by phenotypic or functional markers.

Comparing our results to the Ahmed lab's definitions, the timing and the all-encompassing activation and proliferation of dengue-tetramer^{+} T cells seen during the acute stage of dengue infection would sync up with the effector phase in the YFV vaccine studies. The bifurcation of CD57^{+} CD127^{-} cells and CD127^{+} CD57^{-} cells seen in our study would therefore occur during the transition from effector to memory T cells. The upregulation of CD45RA and persistence of these populations one year after infection also implies that these cells have become memory cells. Hence, we believe that the CD57^{+} CD127^{-} are memory cells that retain effector and senescence characteristics and that CD127^{+} CD57^{-} cells are proliferation-capable memory cells.

In the first cohort, CD57^{+} CD127^{-} cells outnumber CD127^{+} CD57^{-} cells during the early convalescence time point but in the second cohort, CD127^{+} CD57^{-} frequencies are higher than CD57^{+} CD127^{-} cells at the late convalescence and late time points. This sequence of population changes would fit with the theory that rapid expansion of CD57^{+} CD127^{-} effector cells allows them to peak first, followed by their replicative senescence and the slower expansion of the CD127^{+} CD57^{-} memory cells.

The long-term maintenance of CD57^{+} CD127^{-} and CD127^{+} CD57^{-} dengue-specific T cells past one year, their anti-viral capacities upon subsequent DENV infection, and how the immune milieu in acute disease affects their differentiation decisions remain to be determined and may have important implications for vaccine design. Vaccination should ideally elicit memory CD8^{+} T cells that can survive long-term in the absence of antigen and are capable of rapidly mounting an

anti-viral response upon natural DENV infection, thereby controlling DENV infection of susceptible cells. Successful flavivirus vaccines like the vaccines for YFV and the tick-borne encephalitis virus (TBEV) generated robust Th1 and Treg responses early on (Aberle et al., 2015; Blom et al., 2013; James et al., 2013) in tandem with our results, which suggest that these can be useful early indicators of a lasting immune memory.

AUTHOR CONTRIBUTIONS

Conceptualization, M.H.Y.C., L.R., and E.W.N.; Methodology, M.H.Y.C, L.R., and E.W.N.; Investigation, M.H.Y.C., M.Q.L, L.R.; Software, E.B., E.W.N., B.L.; Validation, A.R., M.Q.L., L.R., K.F.; Formal Analysis, M.H.Y.C., B.L., J.M.C.; Resources, L.R., K.F., P.A.M., D.C.L., Y.S.L., E.W.N.; Writing, M.H.Y.C., L.R., E.W.N.; Visualization, M.H.Y.C., J.M.C; Supervision, L.R., E.W.N.; Project Administration, L.R., E.W.N.; Funding Acquisition, L.R., E.W.N.

ACKNOWLEDGEMENTS

The authors thank Dr Brendon Hanson's team for HLA typing of patient samples. We thank Loh Chiew Yee, Chen Xiao Yang, Nicholas Ang, and Esther Mok for assistance in preparing reagents and performing experiments and Emmanuelle Kumaran for assistance in PBMC isolation. We also thank Alessandro Sette for providing some peptides used for preliminary analysis. This work was supported by the SIgN immune monitoring platform (E.W.N.), SIgN core funding (E.W.N.), Singapore NMRC New Investigator grant (L.R.) and by a NMRC Open Fund – Individual Research Grant (L.R.). The LNA cohort study was funded by a grant from MSD International GmbH and Merck Sharp & Dohme Corp. We would like to acknowledge the support from Bing Lim from MSD, and Danilo Casimiro and Kalpit Vora from Merck in enabling this cohort study.

DECLARATION OF INTERESTS

E.W.N. is a board director and shareholder of immunoSCAPE Pte. Ltd., which is an immune profiling service provider. All other authors declare no competing financial interests.

FIGURE LEGENDS

Figure 1. Broad changes in immune cells and plasma cytokines over the course of dengue infection.

(A) UMAP was performed on a combined data set from 14 samples (3 patients X 3 time points, 2 healthy controls) with a maximum of 60,000 live $CD45^+$ $CD14^-$ immune cells per sample and the resulting clusters were identified. (B) Heatmap showing frequency of cells with positive marker expression in each of the identified clusters. (C) Representative UMAP plots from 1 patient with $Ki67^+$ cells (pseudocolor) overlaid over $Ki67^-$ cells (grey). (D) Frequencies of $Ki67^+$ cells in respective immune subsets at acute, post-febrile, and early convalescent time points. See Fig S1A for gating strategies. (E) Log_{10} transformed plasma cytokine concentrations at each time point.

Figure 2. In-depth analysis of $CD4^+$ T cell subsets shows activation and proliferation only during the acute stage of dengue infection.

(A) UMAP was performed on a combined data set of 14 samples with a maximum of 10,000 $CD4^+$ T cells per sample. Clusters were identified by Phenograph clustering. (B) Heatmap of median expression intensities in $CD4^+$ T cell clusters. (C) Frequencies of $CD4^+$ T cell subsets at each time point. See Fig S2 for gating strategies. (D) Frequencies of $Ki67^+$ cells within each $CD4^+$ T cell subset identified in Fig 2C. (E) Frequencies of $CD4^+$ T cells expressing activation markers. (F) Frequencies of Th1 and Treg cells expressing trafficking and activation markers.

Figure 3. In-depth analysis of $CD8^+$ T cells, unconventional T cells, NK, and B cells also shows activation and proliferation only during the acute stage of dengue infection.

(A) UMAP was performed on a combined data set of 14 samples with a maximum of 10,000 $CD8^+$ T cells per sample. Clusters were identified by Phenograph clustering. (B) Heatmap of median expression intensities in $CD8^+$ T cell clusters. (C) Frequencies of $CD8^+$ T cell subsets at each time point. (D) Frequencies of $Ki67^+$ cells within each $CD8^+$ T cell subset identified in Fig 3C. (E) Frequencies of $CD8^+$ T cells expressing activation and trafficking markers. (F) Frequencies of EM cells expressing CCR4 and CCR5. Frequencies of (G) MAIT cells, (H) $\gamma\delta$ T cells, (I) NK cells, (J) NK cell subsets, and (K) B cells expressing activation markers.

Figure 4. Peptide-HLA tetramer screening enables accurate characterization of dengue-specific $CD8^+$ T cells by epitope.

(A) Representative FACS plot of positive tetramer staining. (B) Frequency of Dengue $tetramer^+$ T cells by HLA type and by epitope at each time point. (C) Spearman's correlation between frequency of total dengue $tetramer^+$ T cells at post-febrile and early convalescent time points. (D) Number of patients that responded to each epitope. Related epitopes are indicated in red and green. (E) UMAP was performed on a combined data set of $tetramer^+$ T cells from 28 samples (10 patients x 3 time points and 2 healthy controls) with a maximum of 500 $tetramer^+$ cells per disease per sample. Cells are color coded by disease epitope and stage of dengue infection. (F, G) UMAP was performed on a combined data set of early convalescent stage dengue $tetramer^+$ T cells from 28 samples with a maximum of 1192 cells per sample. Cells are color coded by (F)

HLA type and (G) PD-1 expression intensity. (H) Frequency of early convalescent stage dengue tetramer$^+$ T cells that are PD-1$^+$ by HLA type and dominance status. Each point represents a unique epitope.

Figure 5. Disease-specific analysis of tetramer$^+$ CD8$^+$ T cells.

(A) Mean frequencies of marker-expressing cells within dengue, EBV, and flu tetramer$^+$ T cells, as well as naïve, CM, EM, EMRA, and Ki67$^+$ tetramer-negative T cells, summarized as a heatmap. (B) Frequency of dengue tetramer$^+$ T cells that express the respective activation markers at each time point. (C) Frequency of early convalescent dengue, EBV, and flu tetramer$^+$ T cells that express the respective activation markers.

Figure 6. Dengue tetramer$^+$ T cells differentiate into two different populations.

Monocle 2 trajectory analysis was performed on a combined data set of dengue tetramer$^+$ T cells from 12 samples (4 patients X 3 time points). (A) Monocle plot displays dengue tetramer$^+$ T cells coded by disease stage and branching into two cell fates. (B) Heatmap of marker expression intensity along the Pre-branch, Cell Fate 1, and Cell Fate 2 branches. Cluster 1 shows increasing expression for both cell fates. Cluster 2 shows increasing expression only for Cell Fate 1. Cluster 3 shows increasing expressing only for Cell Fate 2. Cluster 4 shows decreasing expression for both cell fates. (C) Monocle plot showing intensity of CD57 (left) and CD127 (right) expression. (D) Representative FACS plot of dengue, EBV, and flu tetramer$^+$ T cells from one patient. (E) Frequencies of CD57 CD127 subsets within dengue tetramer$^+$ CD8$^+$ cells over time. (F) Memory

subsets within early convalescent epitope tetramer$^+$ cells.

Figure 7. Analysis of a second cohort of dengue patients confirms initial findings.

(A) Frequency of late convalescent dengue tetramer$^+$ T cells that are ICOS$^+$ and PD-1$^+$. (B) Frequency of acute dengue tetramer$^+$ T cells that are CD39$^+$, CD69$^+$, and GPR56$^+$. (C) Monocle 2 trajectory analysis was performed on a combined data set of dengue tetramer$^+$ T cells from 65 samples (22 patients X up to 4 time points). Monocle plot displays dengue tetramer$^+$ T cells coded by disease stage and branching into three cell fates. Arrows indicate direction of time. (D) Heatmap of changing marker expression intensity along the 4 terminal branches. Arrow indicates direction of time for each branch. (E) Monocle plot showing intensity of CD57 (top left), CD127 (top right), CXCR3 (bottom left), and Granzyme B (bottom right) expression. (F) Frequencies of CD57 CD127 subsets within dengue tetramer$^+$ CD8$^+$ cells over time.

Figure S1. Broad changes in immune cells and cytokines. (Related to Figure 1)

(A) Representative FACS plots of gating strategies for main $CD45^+$ $CD14^-$ populations. MAIT ($CD3^+$ $V\alpha7.2^+$ $CD161^+$), $CD4^+$ T ($CD3^+$ $MAIT^-$ $CD4^+$ $CD8^-$), $CD8^+$ T ($CD3^+$ $MAIT^-$ $CD8^+$ $CD4^-$), $V\delta1^+$ $\gamma\delta$ T ($CD3^+$ $MAIT^-$ $TCR\gamma\delta^+$ $V\delta1^+$), $V\delta2^+$ $\gamma\delta$ T ($CD3^+$ $MAIT^-$ $TCR\gamma\delta^+$ $V\delta2^+$), NK ($CD3^-$ $CD56^+$), B ($CD3^-$ $CD56^-$ $CD16^-$ $CD19/CD20^+$ $CXCR5^+$), $CXCR5^-$ B ($CD3^-$ $CD56^-$ $CD16^-$ $CXCR5^-$ $CD38^+$), Plasmablast ($CD3^-$ $CD56^-$ $CD16^-$ $CXCR5^-$ CD38hi). (B) Frequencies of immune cell subsets at the different stages of dengue infection. (C) PCA of plasma cytokine concentrations, coded by different stages of infection.

Figure S2. Analysis of bulk T cells. (Related to Figures 2 and 3)

(A) Heatmap of Jensen-Shannon Divergence indices calculated based on UMAP embeddings from the UMAP plots in Fig 2A and Fig 3A. (B-E) Representative FACS plots of gating strategies for $CD4^+$ subsets. (B) Naive ($CD45RA^+$ $CD45RO^-$ $CCR7^+$), EMRA ($CD45RA^+$ $CD45RO^-$ $CCR7^-$), CM ($CD45RA^-$ $CD45RO^+$ $CCR7^+$), EM ($CD45RA^-$ $CD45RO^+$ $CCR7^-$). (C, clockwise) Th1 ($CXCR3^+$ $CCR6^-$ $Helios^-$ $CXCR5^-$), Th1-like TFH ($CXCR3^+$ $CCR6^-$ $Helios^-$ $CXCR5^+$), Th1Th17 ($CXCR3^+$ $CCR6^+$ $CCR4^-$ $CXCR5^-$), Th17 ($CXCR3^-$ $CCR6^+$ $CCR4^+$ $CXCR5^-$), $CD57^-$ Cytotoxic ($CXCR3^-$ $CCR6^-$ Granzyme B^+ $CD57^-$), $CD57^+$ Cytotoxic ($CXCR3^-$ $CCR6^-$ Granzyme B^+ $CD57^+$), Th2 ($CXCR3^-$ $CCR6^-$ $CCR4^+$ $GATA3^+$). (D) TFH ($CXCR5^+$ $CXCR3^-$ $Helios^-$). (E) Treg ($FOXP3^+$ $CD25^+$ $CD127^-$). (F) Representative FACS plots of gating strategies for T cell activation markers. Top left to right. $CD38^+$ $CCR7^-$, $CD69^+$, $CCR5^+$ and $TBET^+$. Bottom left to right. $ICOS^+$ $PD\text{-}1^+$, $Ki67^+$, CLA^+. (G) Frequencies of CCR4 and Ki67 subsets in $CD4^+$ T cells. (H) $CCR4^+$ $CD4^+$ cells are $FOXP3^+$ and $CD45RO^+$ compared to total $CD4^+$ population.

Figure S3. PCA of broad immune subset frequencies (Related to Figures 2 and 3 and Table S3)

(A) PCA graph. Only samples with more than one time point are shown. Time points from the same individual are connected by lines colored by the predicted disease status. (B, C) PCA loadings for PC1 and PC2.

Figure S4. Analysis of tetramer$^+$ T cells (Related to Figure 4)

(A) FACS plots of hits $M_{255-263}$ (AYTIGTTYF) and $M_{261-269}$ (TYFQRVLIF). (B) UMAP was performed on a combined data set of tetramer$^+$ T cells and tetramer-negative CD8$^+$ T cells from 28 samples (10 patients X 3 time points and 2 healthy controls) with a maximum of 2200 cells per disease per sample. UMAP plots display (Left) tetramer$^+$ cells coded by disease and stage of dengue infection, overlaid over tetramer-negative cells and (Right) intensity of CCR7, CD45RA, and CD45RO expression. (C-E) UMAP plots as in Fig 4E displaying (C) expression intensities of important markers Ki67, CD57, and CD127, (D) HLA type of bound tetramer, and (E) dominance of dengue epitopes. (F) Representative FACS plot of Granzyme B$^+$ CD57$^+$ CD8$^+$ T cells in healthy control.

Figure S5. Tetramer frequencies and diversities in individual patients. (Related to Figure 4)

(A) (Top rows) Frequency of tetramer staining compared with ELISPOT results from stimulation with peptide hits for each patient. (Bottom rows) Diversity of hits within each patient. (B) Heatmap of Jensen-Shannon Divergence indices calculated based on UMAP embeddings from the UMAP plot in Fig 4E. (C) Number of antigens detected per patient. (D) Tetramer$^+$ T cells and IFN-γ ELISPOT results by HLA type.

Figure S6. Network map of significant associations between immune parameters from the acute and early convalescent stages of dengue infection. (Related to Figure 6)

Parameters from the acute stage (V1) are pink while parameters from the early convalescent stage (V3) are blue. Broad subsets are coded as ellipses, dengue T cell subsets as rectangles, and cytokines as diamonds. Edge width is proportional to Spearman's rho^2 value. Grey lines indicate associations that are positively correlated and red lines indicate associations that are negatively correlated.

TABLE LEGENDS

Table S1. Clinical details of patient samples and Mab and LNA cohorts.

Table S2. Mass cytometry staining panels, experiment batches, and tetramers used.

Table S3. Broad immune cell analysis

Table S4. Cytokine Luminex analysis

Table S5. Tetramer Hits. Antigens highlighted in green are unreported variants of known antigens and antigens highlighted in yellow do not have any variants reported in the Immune Epitope Database.

Table S6. Analysis that compares immune parameters from the acute and early convalescent stages of dengue infection.

REFERENCES

Aberle, J.H., Schwaiger, J., Aberle, S.W., Stiasny, K., Scheinost, O., Kundi, M., Chmelik, V., and Heinz, F.X. (2015). Human CD4+ T Helper Cell Responses after Tick-Borne Encephalitis Vaccination and Infection. PLOS ONE *10*, e0140545.

Acosta-Rodriguez, E.V., Rivino, L., Geginat, J., Jarrossay, D., Gattorno, M., Lanzavecchia, A., Sallusto, F., and Napolitani, G. (2007). Surface phenotype and antigenic specificity of human interleukin 17–producing T helper memory cells. Nat. Immunol. *8*, 639–646.

Akondy, R.S., Monson, N.D., Miller, J.D., Edupuganti, S., Teuwen, D., Wu, H., Quyyumi, F., Garg, S., Altman, J.D., Rio, C.D., et al. (2009). The Yellow Fever Virus Vaccine Induces a Broad and Polyfunctional Human Memory CD8+ T Cell Response. J. Immunol. *183*, 7919–7930.

Akondy, R.S., Johnson, P.L.F., Nakaya, H.I., Edupuganti, S., Mulligan, M.J., Lawson, B., Miller, J.D., Pulendran, B., Antia, R., and Ahmed, R. (2015). Initial viral load determines the magnitude of the human CD8 T cell response to yellow fever vaccination. Proc. Natl. Acad. Sci. *112*, 3050–3055.

Akondy, R.S., Fitch, M., Edupuganti, S., Yang, S., Kissick, H.T., Li, K.W., Youngblood, B.A., Abdelsamed, H.A., McGuire, D.J., Cohen, K.W., et al. (2017). Origin and differentiation of human memory CD8 T cells after vaccination. Nature *552*, 362.

de Alwis, R., Bangs, D.J., Angelo, M.A., Cerpas, C., Fernando, A., Sidney, J., Peters, B., Gresh, L., Balmaseda, A., Silva, A.D. de, et al. (2016). Immunodominant Dengue Virus-Specific CD8+ T Cell Responses Are Associated with a Memory PD-1+ Phenotype. J. Virol. *90*, 4771–4779.

Bachelerie, F., Ben-Baruch, A., Burkhardt, A.M., Combadiere, C., Farber, J.M., Graham, G.J., Horuk, R., Sparre-Ulrich, A.H., Locati, M., Luster, A.D., et al. (2014). International Union of Basic and Clinical Pharmacology. LXXXIX. Update on the Extended Family of Chemokine Receptors and Introducing a New Nomenclature for Atypical Chemokine Receptors. Pharmacol. Rev. *66*, 1–79.

Becht, E., McInnes, L., Healy, J., Dutertre, C.-A., Kwok, I.W.H., Ng, L.G., Ginhoux, F., and Newell, E.W. (2018a). Dimensionality reduction for visualizing single-cell data using UMAP. Nat. Biotechnol.

Becht, E., Simoni, Y., Coustan-Smith, E., Maximilien, E., Cheng, Y., Ng, L.G., Campana, D., Newell, E., and Wren, J. (2018b). Reverse-engineering flow-cytometry gating strategies for phenotypic labelling and high-performance cell sorting. Bioinformatics.

Bengsch, B., Ohtani, T., Herati, R.S., Bovenschen, N., Chang, K.-M., and Wherry, E.J. (2018). Deep immune profiling by mass cytometry links human T and NK cell differentiation and cytotoxic molecule expression patterns. J. Immunol. Methods *453*, 3–10.

Bhatt, S., Gething, P.W., Brady, O.J., Messina, J.P., Farlow, A.W., Moyes, C.L., Drake, J.M., Brownstein, J.S., Hoen, A.G., Sankoh, O., et al. (2013). The global distribution and burden of dengue. Nature *496*, 504–507.

Blom, K., Braun, M., Ivarsson, M.A., Gonzalez, V.D., Falconer, K., Moll, M., Ljunggren, H.-G., Michaëlsson, J., and Sandberg, J.K. (2013). Temporal Dynamics of the Primary Human T Cell Response to Yellow Fever Virus 17D As It Matures from an Effector- to a Memory-Type Response. J. Immunol. *190*, 2150–2158.

Brenchley, J.M., Karandikar, N.J., Betts, M.R., Ambrozak, D.R., Hill, B.J., Crotty, L.E., Casazza, J.P., Kuruppu, J., Migueles, S.A., Connors, M., et al. (2003). Expression of CD57 defines replicative senescence and antigen-induced apoptotic death of CD8+ T cells. Blood *101*, 2711–2720.

Cellerai, C., Perreau, M., Rozot, V., Enders, F.B., Pantaleo, G., and Harari, A. (2010). Proliferation Capacity and Cytotoxic Activity Are Mediated by Functionally and Phenotypically Distinct Virus-Specific CD8 T Cells Defined by Interleukin-7Rα (CD127) and Perforin Expression. J. Virol. *84*, 3868–3878.

Chandele, A., Sewatanon, J., Gunisetty, S., Singla, M., Onlamoon, N., Akondy, R.S., Kissick, H.T., Nayak, K., Reddy, E.S., Kalam, H., et al. (2016). Characterization of Human CD8 T Cell Responses in Dengue Virus-Infected Patients from India. J. Virol. *90*, 11259–11278.

Chattopadhyay, P.K., Betts, M.R., Price, D.A., Gostick, E., Horton, H., Roederer, M., and Rosa, S.C.D. (2009). The cytolytic enzymes granyzme A, granzyme B, and perforin: expression patterns, cell distribution, and their relationship to cell maturity and bright CD57 expression. J. Leukoc. Biol. *85*, 88–97.

Conroy, A.L., Gélvez, M., Hawkes, M., Rajwans, N., Tran, V., Liles, W.C., Villar-Centeno, L.A., and Kain, K.C. (2015). Host biomarkers are associated with progression to dengue haemorrhagic fever: a nested case-control study. Int. J. Infect. Dis. *40*, 45–53.

Duangchinda, T., Dejnirattisai, W., Vasanawathana, S., Limpitikul, W., Tangthawornchaikul, N., Malasit, P., Mongkolsapaya, J., and Screaton, G. (2010). Immunodominant T-cell responses to dengue virus NS3 are associated with DHF. Proc. Natl. Acad. Sci. *107*, 16922–16927.

Dung, N.T.P., Duyen, H.T.L., Thuy, N.T.V., Ngoc, T.V., Chau, N.V.V., Hien, T.T., Rowland-Jones, S.L., Dong, T., Farrar, J., Wills, B., et al. (2010). Timing of CD8+ T Cell Responses in Relation to Commencement of Capillary Leakage in Children with Dengue. J. Immunol. *184*, 7281–7287.

Friberg, H., Bashyam, H., Toyosaki-Maeda, T., Potts, J.A., Greenough, T., Kalayanarooj, S., Gibbons, R.V., Nisalak, A., Srikiatkhachorn, A., Green, S., et al. (2011). Cross-Reactivity and Expansion of Dengue-Specific T cells During Acute Primary and Secondary Infections in Humans. Sci. Rep. *1*, 51.

Gattinoni, L., Lugli, E., Ji, Y., Pos, Z., Paulos, C.M., Quigley, M.F., Almeida, J.R., Gostick, E., Yu, Z., Carpenito, C., et al. (2011). A human memory T cell subset with stem cell–like properties. Nat. Med. *17*, 1290–1297.

Gebhardt, T., Wakim, L.M., Eidsmo, L., Reading, P.C., Heath, W.R., and Carbone, F.R. (2009). Memory T cells in nonlymphoid tissue that provide enhanced local immunity during infection with herpes simplex virus. Nat. Immunol. *10*, 524–530.

Gosselin, A., Monteiro, P., Chomont, N., Diaz-Griffero, F., Said, E.A., Fonseca, S., Wacleche, V., El-Far, M., Boulassel, M.-R., Routy, J.-P., et al. (2010). Peripheral Blood CCR4+CCR6+ and CXCR3+CCR6+ CD4+ T Cells Are Highly Permissive to HIV-1 Infection. J. Immunol. *184*, 1604–1616.

Green, S., Pichyangkul, S., Vaughn, D.W., Kalayanarooj, S., Nimmannitya, S., Nisalak, A., Kurane, I., Rothman, A.L., and Ennis, F.A. (1999). Early CD69 Expression on Peripheral Blood Lymphocytes from Children with Dengue Hemorrhagic Fever. J. Infect. Dis. *180*, 1429–1435.

Guzmán, M.G., Kouri, G.P., Bravo, J., Soler, M., Vazquez, S., and Morier, L. (1990). Dengue Hemorrhagic Fever in Cuba, 1981: A Retrospective Seroepidemiologic Study. Am. J. Trop. Med. Hyg. *42*, 179–184.

Her, Z., Kam, Y.-W., Gan, V.C., Lee, B., Thein, T.-L., Tan, J.J.L., Lee, L.K., Fink, K., Lye, D.C., Rénia, L., et al. (2017). Severity of Plasma Leakage Is Associated With High Levels of Interferon γ–Inducible Protein 10, Hepatocyte Growth Factor, Matrix Metalloproteinase 2 (MMP-2), and MMP-9 During Dengue Virus Infection. J. Infect. Dis. *215*, 42–51.

Hsieh, M.-F., Lai, S.-L., Chen, J.-P., Sung, J.-M., Lin, Y.-L., Wu-Hsieh, B.A., Gerard, C., Luster, A., and Liao, F. (2006). Both CXCR3 and CXCL10/IFN-Inducible Protein 10 Are Required for Resistance to Primary Infection by Dengue Virus. J. Immunol. *177*, 1855–1863.

Huang, J., Liang, W., Chen, S., Zhu, Y., Chen, H., Mok, C.K.P., and Zhou, Y. (2018). Serum Cytokine Profiles in Patients with Dengue Fever at the Acute Infection Phase. Dis. Markers *2018*, 8403937.

Ibegbu, C.C., Xu, Y.-X., Harris, W., Maggio, D., Miller, J.D., and Kourtis, A.P. (2005). Expression of Killer Cell Lectin-Like Receptor G1 on Antigen-Specific Human CD8+ T Lymphocytes during Active, Latent, and Resolved Infection and its Relation with CD57. J. Immunol. *174*, 6088–6094.

James, E.A., LaFond, R.E., Gates, T.J., Mai, D.T., Malhotra, U., and Kwok, W.W. (2013). Yellow Fever Vaccination Elicits Broad Functional CD4+ T Cell Responses That Recognize Structural and Nonstructural Proteins. J. Virol. *87*, 12794–12804.

Jayaratne, H.E., Wijeratne, D., Fernando, S., Kamaladasa, A., Gomes, L., Wijewickrama, A., Ogg, G.S., and Malavige, G.N. (2018). Regulatory T-cells in acute dengue viral infection. Immunology *154*, 89–97.

Kaech, S.M., Tan, J.T., Wherry, E.J., Konieczny, B.T., Surh, C.D., and Ahmed, R. (2003). Selective expression of the interleukin 7 receptor identifies effector CD8 T cells that give rise to long-lived memory cells. Nat. Immunol. *4*, 1191–1198.

Keawvichit, R., Khowawisetsut, L., Lertjuthaporn, S., Tangnararatchakit, K., Apiwattanakul, N., Yoksan, S., Chuansumrit, A., Chokephaibulkit, K., Ansari, A.A., Onlamoon, N., et al. (2018). Differences in activation and tissue homing markers of natural killer cell subsets during acute dengue infection. Immunology *153*, 455–465.

Kunicki, M.A., Hernandez, L.C.A., Davis, K.L., Bacchetta, R., and Roncarolo, M.-G. (2017). Identity and Diversity of Human Peripheral Th and T Regulatory Cells Defined by Single-Cell Mass Cytometry. J. Immunol. ji1701025.

van Leeuwen, E.M.M., Bree, G.J. de, Remmerswaal, E.B.M., Yong, S.-L., Tesselaar, K., Berge, I.J.M. ten, and Lier, R.A.W. van (2005). IL-7 receptor α chain expression distinguishes functional subsets of virus-specific human CD8+ T cells. Blood *106*, 2091–2098.

Levine, J.H., Simonds, E.F., Bendall, S.C., Davis, K.L., Amir, E.D., Tadmor, M.D., Litvin, O., Fienberg, H.G., Jager, A., Zunder, E.R., et al. (2015). Data-Driven Phenotypic Dissection of AML Reveals Progenitor-like Cells that Correlate with Prognosis. Cell *162*, 184–197.

Lühn, K., Simmons, C.P., Moran, E., Dung, N.T.P., Chau, T.N.B., Quyen, N.T.H., Thao, L.T.T., Ngoc, T.V., Dung, N.M., Wills, B., et al. (2007). Increased frequencies of CD4+CD25high regulatory T cells in acute dengue infection. J. Exp. Med. *204*, 979–985.

McInnes, L., and Healy, J. (2018). UMAP: Uniform Manifold Approximation and Projection for Dimension Reduction. ArXiv180203426 Cs Stat.

Messina, J.P., Brady, O.J., Scott, T.W., Zou, C., Pigott, D.M., Duda, K.A., Bhatt, S., Katzelnick, L., Howes, R.E., Battle, K.E., et al. (2014). Global spread of dengue virus types: mapping the 70 year history. Trends Microbiol. *22*, 138–146.

Metzemaekers, M., Vanheule, V., Janssens, R., Struyf, S., and Proost, P. (2018). Overview of the Mechanisms that May Contribute to the Non-Redundant Activities of Interferon-Inducible CXC Chemokine Receptor 3 Ligands. Front. Immunol. *8*.

Miller, J.D., Most, R.G. van der, Akondy, R.S., Glidewell, J.T., Albott, S., Masopust, D., Murali-Krishna, K., Mahar, P.L., Edupuganti, S., Lalor, S., et al. (2008). Human Effector and Memory CD8+ T Cell Responses to Smallpox and Yellow Fever Vaccines. Immunity *28*, 710–722.

Mongkolsapaya, J., Dejnirattisai, W., Xu, X., Vasanawathana, S., Tangthawornchaikul, N., Chairunsri, A., Sawasdivorn, S., Duangchinda, T., Dong, T., Rowland-Jones, S., et al. (2003). Original antigenic sin and apoptosis in the pathogenesis of dengue hemorrhagic fever. Nat. Med. *9*, 921–927.

Mongkolsapaya, J., Duangchinda, T., Dejnirattisai, W., Vasanawathana, S., Avirutnan, P., Jairungsri, A., Khemnu, N., Tangthawornchaikul, N., Chotiyarnwong, P., Sae-Jang, K., et al. (2006). T Cell Responses in Dengue Hemorrhagic Fever: Are Cross-Reactive T Cells Suboptimal? J. Immunol. *176*, 3821–3829.

Napolitani, G., Kurupati, P., Teng, K.W.W., Gibani, M.M., Rei, M., Aulicino, A., Preciado-Llanes, L., Wong, M.T., Becht, E., Howson, L., et al. (2018). Clonal analysis of Salmonella -specific effector T cells reveals serovar-specific and cross-reactive T cell responses. Nat. Immunol. *19*, 742–754.

Newell, E.W., Sigal, N., Nair, N., Kidd, B.A., Greenberg, H.B., and Davis, M.M. (2013). Combinatorial tetramer staining and mass cytometry analysis facilitate T-cell epitope mapping and characterization. Nat. Biotechnol. *31*, 623–629.

Paquin-Proulx, D., Avelino-Silva, V.I., Santos, B.A.N., Barsotti, N.S., Siroma, F., Ramos, J.F., Tonacio, A.C., Song, A., Maestri, A., Cerqueira, N.B., et al. (2018). MAIT cells are activated in acute Dengue virus infection and after in vitro Zika virus infection. PLoS Negl. Trop. Dis. *12*, e0006154.

Paul, S., Weiskopf, D., Angelo, M.A., Sidney, J., Peters, B., and Sette, A. (2013). HLA Class I Alleles Are Associated with Peptide-Binding Repertoires of Different Size, Affinity, and Immunogenicity. J. Immunol. *191*, 5831–5839.

Petitdemange, C., Wauquier, N., Devilliers, H., Yssel, H., Mombo, I., Caron, M., Nkoghé, D., Debré, P., Leroy, E., and Vieillard, V. (2016). Longitudinal Analysis of Natural Killer Cells in Dengue Virus-Infected Patients in Comparison to Chikungunya and Chikungunya/Dengue Virus-Infected Patients. PLoS Negl. Trop. Dis. *10*, e0004499.

Priol, Y.L., Puthier, D., Lécureuil, C., Combadière, C., Debré, P., Nguyen, C., and Combadière, B. (2006). High Cytotoxic and Specific Migratory Potencies of Senescent CD8+CD57+ Cells in HIV-Infected and Uninfected Individuals. J. Immunol. *177*, 5145–5154.

Qiu, X., Mao, Q., Tang, Y., Wang, L., Chawla, R., Pliner, H.A., and Trapnell, C. (2017). Reversed graph embedding resolves complex single-cell trajectories. Nat. Methods *14*, 979.

Rathakrishnan, A., Wang, S.M., Hu, Y., Khan, A.M., Ponnampalavanar, S., Lum, L.C.S., Manikam, R., and Sekaran, S.D. (2012). Cytokine Expression Profile of Dengue Patients at Different Phases of Illness. PLoS ONE *7*.

Rivino, L., Kumaran, E.A.P., Jovanovic, V., Nadua, K., Teo, E.W., Pang, S.W., Teo, G.H., Gan, V.C.H., Lye, D.C., Leo, Y.S., et al. (2013). Differential Targeting of Viral Components by CD4+ versus CD8+ T Lymphocytes in Dengue Virus Infection. J. Virol. *87*, 2693–2706.

Rivino, L., Kumaran, E.A., Thein, T.-L., Too, C.T., Gan, V.C.H., Hanson, B.J., Wilder-Smith, A., Bertoletti, A., Gascoigne, N.R.J., Lye, D.C., et al. (2015). Virus-specific T lymphocytes home to the skin during natural dengue infection. Sci. Transl. Med. *7*, 278ra35-278ra35.

Sallusto, F., Lenig, D., Förster, R., Lipp, M., and Lanzavecchia, A. (1999). Two subsets of memory T lymphocytes with distinct homing potentials and effector functions. Nature *401*, 708–712.

Simmons, C.P., Dong, T., Chau, N.V., Dung, N.T.P., Chau, T.N.B., Thao, L.T.T., Dung, N.T., Hien, T.T., Rowland-Jones, S., and Farrar, J. (2005). Early T-Cell Responses to Dengue Virus Epitopes in Vietnamese Adults with Secondary Dengue Virus Infections. J. Virol. *79*, 5665–5675.

Simoni, Y., Becht, E., Fehlings, M., Loh, C.Y., Koo, S.-L., Teng, K.W.W., Yeong, J.P.S., Nahar, R., Zhang, T., Kared, H., et al. (2018). Bystander CD8 + T cells are abundant and phenotypically distinct in human tumour infiltrates. Nature *557*, 575–579.

Sridhar, S., Luedtke, A., Langevin, E., Zhu, M., Bonaparte, M., Machabert, T., Savarino, S., Zambrano, B., Moureau, A., Khromava, A., et al. (2018). Effect of Dengue Serostatus on Dengue Vaccine Safety and Efficacy. N. Engl. J. Med. *379*, 327–340.

St John, A.L., and Rathore, A.P.S. (2019). Adaptive immune responses to primary and secondary dengue virus infections. Nat. Rev. Immunol. 1.

Sugiyama, D., Nishikawa, H., Maeda, Y., Nishioka, M., Tanemura, A., Katayama, I., Ezoe, S., Kanakura, Y., Sato, E., Fukumori, Y., et al. (2013). Anti-CCR4 mAb selectively depletes effector-type FoxP3+CD4+ regulatory T cells, evoking antitumor immune responses in humans. Proc. Natl. Acad. Sci. *110*, 17945–17950.

Tian, Y., Babor, M., Lane, J., Schulten, V., Patil, V.S., Seumois, G., Rosales, S.L., Fu, Z., Picarda, G., Burel, J., et al. (2017). Unique phenotypes and clonal expansions of human CD4 effector memory T cells re-expressing CD45RA. Nat. Commun. *8*, 1473.

Tian, Y., Babor, M., Lane, J., Seumois, G., Liang, S., Goonawardhana, N.D.S., Silva, A.D.D., Phillips, E.J., Mallal, S.A., Antunes, R. da S., et al. (2019). Dengue-specific $CD8^+$ T cell subsets display specialized transcriptomic and TCR profiles. J. Clin. Invest. *129*, 1727–1741.

Townsley, E., Woda, M., Thomas, S.J., Kalayanarooj, S., Gibbons, R.V., Nisalak, A., Srikiatkhachorn, A., Green, S., Stephens, H.A., Rothman, A.L., et al. (2014). Distinct activation phenotype of a highly conserved novel HLA-B57-restricted epitope during dengue virus infection. Immunology *141*, 27–38.

Treiner, E., Duban, L., Bahram, S., Radosavljevic, M., Wanner, V., Tilloy, F., Affaticati, P., Gilfillan, S., and Lantz, O. (2003). Selection of evolutionarily conserved mucosal-associated invariant T cells by MR1. Nature *422*, 164–169.

Tsai, C.-Y., Liong, K.H., Gunalan, M.G., Li, N., Lim, D.S.L., Fisher, D.A., MacAry, P.A., Leo, Y.S., Wong, S.-C., Puan, K.J., et al. (2015). Type I IFNs and IL-18 Regulate the Antiviral Response of Primary Human γδ T Cells against Dendritic Cells Infected with Dengue Virus. J. Immunol. *194*, 3890–3900.

Vaughn, D.W., Green, S., Kalayanarooj, S., Innis, B.L., Nimmannitya, S., Suntayakorn, S., Rothman, A.L., Ennis, F.A., and Nisalak, A. (1997). Dengue in the early febrile phase: viremia and antibody responses. J. Infect. Dis. *176*, 322–330.

Vermijlen, D., Gatti, D., Kouzeli, A., Rus, T., and Eberl, M. (2018). γδ T cell responses: How many ligands will it take till we know? Semin. Cell Dev. Biol.

Weiskopf, D., Angelo, M.A., Azeredo, E.L. de, Sidney, J., Greenbaum, J.A., Fernando, A.N., Broadwater, A., Kolla, R.V., Silva, A.D.D., Silva, A.M. de, et al. (2013). Comprehensive analysis of dengue virus-specific responses supports an HLA-linked protective role for CD8+ T cells. Proc. Natl. Acad. Sci. *110*, E2046–E2053.

Weiskopf, D., Bangs, D.J., Sidney, J., Kolla, R.V., Silva, A.D.D., Silva, A.M. de, Crotty, S., Peters, B., and Sette, A. (2015). Dengue virus infection elicits highly polarized CX3CR1+ cytotoxic CD4+ T cells associated with protective immunity. Proc. Natl. Acad. Sci. *112*, E4256–E4263.

Wells, R.A., Scott, R.M., Pavanand, K., Sathitsathein, V., Cheamudon, U., and Macdermott, R.P. (1980). Kinetics of peripheral blood leukocyte alterations in Thai children with dengue hemorrhagic fever. Infect. Immun. *28*, 428–433.

van Wilgenburg, B., Scherwitzl, I., Hutchinson, E.C., Leng, T., Kurioka, A., Kulicke, C., de Lara, C., Cole, S., Vasanawathana, S., Limpitikul, W., et al. (2016). MAIT cells are activated during human viral infections. Nat. Commun. *7*, 11653.

Wong, M.T., Chen, J., Narayanan, S., Lin, W., Anicete, R., Kiaang, H.T.K., De Lafaille, M.A.C., Poidinger, M., and Newell, E.W. (2015). Mapping the Diversity of Follicular Helper T Cells in Human Blood and Tonsils Using High-Dimensional Mass Cytometry Analysis. Cell Rep. *11*, 1822–1833.

Wrammert, J., Onlamoon, N., Akondy, R.S., Perng, G.C., Polsrila, K., Chandele, A., Kwissa, M., Pulendran, B., Wilson, P.C., Wittawatmongkol, O., et al. (2012). Rapid and Massive Virus-Specific Plasmablast Responses during Acute Dengue Virus Infection in Humans. J. Virol. *86*, 2911–2918.

Yang, J., Zhu, H., Murphy, T.L., Ouyang, W., and Murphy, K.M. (2001). IL-18–stimulated GADD45β required in cytokine-induced, but not TCR-induced, IFN-γ production. Nat. Immunol. *2*, 157–164.

Zaunders, J.J., Munier, M.L., Kaufmann, D.E., Ip, S., Grey, P., Smith, D., Ramacciotti, T., Quan, D., Finlayson, R., Kaldor, J., et al. (2005). Early proliferation of CCR5+ CD38+++ antigen-specific CD4+ Th1 effector cells during primary HIV-1 infection. Blood *106*, 1660–1667.

MATERIALS AND METHODS

Patients and ethics statement

All patients in the Mab cohort (Table S1) were recruited at Tan Tock Seng Hospital in Singapore during acute dengue infection and blood samples were taken after informed consent at three time points of infection: acute, post-febrile, and early convalescent (days 6-9, 14-21 and 40-80 from fever onset, respectively). Patients were diagnosed by a team of clinicians according to WHO guidelines, as described previously (Rivino et al., 2013). The study was conducted in accordance with the Declaration of Helsinki and approved by the Singapore National Healthcare Group ethical review board (DSRB 2008/00293). Blood from anonymous healthy donors were also collected at the Singapore Immunology Network (SIgN) with approval by the Centralised Institutional Review Board (CIRB 2017/2806). Blood samples were collected in EDTA vacutainer tubes. PBMCs were isolated from peripheral blood by Ficoll gradient purification and cryopreserved in 90% fetal calf serum + 10% DMSO.

All methods for patients in the LNA cohort were identical except for the time points of blood sample collection: acute (days 3-8 from fever onset), post-febrile (days 10-27), late convalescent (days 173-192), and late (days 357-381). The Singapore National Healthcare Group ethical review board number is NHG DSRB 2015/00528.

Antibody and streptavidin labelling

Recombinant streptavidin was expressed and refolded in house as previously described (Cheng et al., 2019; Newell et al., 2013). Purified antibodies without carrier proteins were purchased as

listed in Table S2. Maleimide-conjugated DN3 MAXPAR chelating polymers (Fluidigm) were loaded with heavy metal isotopes (Fluidigm) according to the manufacturer's recommendations. For antibody conjugations, 100 µg of purified antibodies lacking carrier proteins were coupled with the metal polymer structures according to the protocol provided by Fluidigm. For streptavidin conjugations, 100 µg of streptavidin was conjugated to the respective metal-loaded DN3 polymer and finally diluted to a concentration of 200 µg/mL for subsequent tetramerization (Leong and Newell, 2015; Newell et al., 2013).

Virus epitope selection and prediction

DENV and control epitopes for HLA-B*58:01, A*11:01, and A*24:02 were obtained from the IEDB (Vita et al., 2018) and previous papers (Rivino et al., 2013). Serotype variations to cover all 4 DENV serotypes were predicted for these peptides. In addition, 9- and 10-mer peptides based on the sequence of DENV-1 virus (strain TSV08-1-I) and DENV-2 virus (strain TSV01-2) were predicted for their binding affinity to A*11:01 and A*24:02 using the consensus prediction tool on the IEDB website (Vita et al., 2018). For each allele, peptides were selected if they were in the top 0.8% of binders. All peptides were synthesized by Mimotopes (Australia) with purity > 80%.

Peptides sequence similarity and cluster assignment

To avoid incorrect interpretations from cross-reactive T cell epitopes, sequences were loaded onto a Biostrings-based R-written environment (Newell et al., 2013). The biological sequence and matching algorithm performed pairwise alignment to calculate the peptide binding score based

on their sequence similarity and HLA anchor point. Peptides with similar binding scores were assigned the same peptide cluster number. The resulting peptide cluster assignations are listed in Table S2. Peptides within the same cluster were then assigned the same triple SAV-metal codings.

UV peptide exchange to generate pHLA

UV-cleavable peptide HLA monomers were produced in-house as previously described (Cheng et al., 2019; Newell et al., 2013). Peptide exchange was performed at 100 µg/mL of HLA monomer in 100 µL PBS with 25 µM of peptide of interest in a 96-well plate. The mixture was exposed to 365 nm UV irradiation for 2 sessions of 5 minutes using a UVP CL-1000 Ultraviolet Crosslinker, and then stored at 4°C overnight to complete the exchange.

84-plex or 220-plex combinatorial pHLA tetramer production

Each metal-labelled streptavidin was diluted to 25 µg/mL in EDTA-free W buffer. To eliminate false positives from non-specific tetramer staining, two different configurations of triple streptavidin-metal codings were generated. The metal-labeled streptavidins were mixed using an automated liquid distribution robot (TECAN Freedom Evo200). On the day of cell staining, the triple streptavidin-metal mixtures were added to the corresponding pHLA in a stepwise manner of three additions, with 10 min of incubation time at room temperature between each step. Finally, 10 µM D-biotin (Sigma) was added to the tetramerized pHLA complexes to saturate unbound streptavidin. All tetramers for each configuration were combined and concentrated

down to 5 µg/mL per pHLA tetramer in 10% FBS CyFACS buffer using an Amicon Ultra 50 kDa filter (Millipore).

Cell Staining and Mass Cytometry Acquisition

All antibody and tetramer cocktails were prepared on the day of cell staining. Antibodies used for pre-staining (Table S2) were combined in a 30 kDa filter (Amicon Ultra, Millipore), washed and centrifuged with PBS twice to remove azide content. Before staining, all tetramer and antibody cocktails were filtered using a 0.1 µM filter (Ultrafree, Millipore) to remove aggregates. Cryopreserved cells were thawed and washed twice with complete RPMI media (10% FBS, 1% penicillin/streptomycin/L-glutamine) (Gibco, Invitrogen). 80% of the cells were split evenly into two wells for Panel 1 staining with two different tetramer configurations and the remaining 20% of cells were used for staining with Panel 2. Cells were incubated with 50 nM dasatinib and pre-stain antibodies in complete RPMI for 30 min at 37°C. After pre-staining, cells were washed in cold CyFACS buffer (PBS with 4% FCS, 2 mM EDTA, and 0.05% Azide) and incubated on ice with 200 nM Cisplatin (Sigma) for 5 min. Cells were then washed twice with CyFACs and incubated for 1 hour at room temperature with tetramer cocktail. Subsequently, cells were washed and stained with primary surface antibodies and/or EasySep Human T cell Isolation Cocktail (STEMCELL) for 15 min at 4°C. Cells were washed and stained with secondary surface antibodies and/or EasySep Dextran RapidSpheres (STEMCELL) for 15 min at 4°C.

For intracellular and intranuclear antibody staining, cells were washed and fixed with Foxp3/Transcription Factor Fix/Perm buffer (eBiosciences) for 30 min on ice. Cells were then

washed with 1X Permeabilization buffer (eBiosciences) and stained with primary intracellular antibodies for 30 min on ice, washed twice, followed by incubation with secondary intracellular antibodies for 30 min on ice. Finally, cells were washed with 1X Permeabilization buffer and fixed in 2% PFA (paraformaldehyde, Electron Microscopy Science) at 4°C overnight.

On the next day, PFA was removed and cells were incubated with cellular barcodes for 30 min on ice as previously described (Wong et al., 2015). Cells were then washed first with perm buffer, followed by CyFACS. Cellular DNA was labeled at room temperature with 250 nM iridium interchelator (Fluidigm) diluted in 2% PFA for 20 min. Subsequently, cells were washed with CyFACS, combined and enriched for CD3+ T cells using a magnet (EasySep). Immediately before mass cytometry acquisition, cells were washed twice with MilliQ water and passed into a filter top FACS tube. 1.5% of Four EQ beads (Fluidigm DVS) were mixed with the cell suspension. The first two batches of samples were acquired on a CyTOF2 instrument and the third batch of samples was acquired on a Helios instrument.

Mass Cytometry Data Pre-Processing

After mass cytometry acquisition, the signal of each parameter was normalized based on the equilibration beads added to each sample (Finck et al., 2013). All zero values were randomized by an R-script that uniformly distributes values between minus-one and zero. Individual samples were debarcoded manually in FlowJo v10 (Treestar, Inc.). For identification of tetramer positive CD8 cells, live singlet CD8+ T cells were gated and exported individually as CD8 Config 1 and CD8 Config 2 fcs files. Thresholds for each metal-labelled streptavidin channel were manually defined

by gating a CD8+ T cell population that was negative for all of the streptavidin channels and using that as the tetramer negative baseline. Using the tetramer deconvolution algorithm (Newell et al., 2013), only cells positive for above-threshold staining in only three streptavidin channels were considered positive for tetramer staining. Frequencies of tetramer positive cells identified in the two different tetramer coding configurations of the same donor were further calculated for their likely correspondence using statistical stimulation, with $p<0.1$ being considered as plausible detection. Lastly, where there were multiple time points from the same donor, if the concordance in frequency of tetramer+ T cells failed to be achieved at two or more time points, the hit was removed.

High Dimensional Cytometric Data Visualization and Analysis

All data were transformed in R using the "logicleTransform" function by using the "flowCore" package (parameters: w = 0.25, t = 16,409, m = 4.5, a = 0). UMAP dimensionality reduction analysis was carried out using the R package uwot (McInnes and Healy, 2018)(Becht et al., in press). Louvain clustering analyses using Phenograph was used to identify clusters based on marker expression in an automated unbiased fashion (Levine et al., 2015). These clusters were then curated and named according to definitions that have previously been reported in the literature (Acosta-Rodriguez et al., 2007; Gosselin et al., 2010; Kunicki et al., 2017; Weiskopf et al., 2015; Wong et al., 2015). Hypergate was used to identify optimized gating strategies that accurately described these subsets using as few markers as possible (Becht et al., 2018). For this study, optimized gating strategies mostly selected for combinations of surface chemokine receptors, not transcription factors. For simplicity of presentation, we have not appended "-like"

to subsets defined by surface markers. The optimized gating strategies were then applied to the different batches of experiments, with manual changes to account for batch effects, and from there frequencies of the various populations and subsets were identified. The code for calculating Jensen Shannon Distances was adapted from the R package cytutils (Amir, 2019)

For Monocle 2 analysis (Qiu et al., 2017), the dataset of marker intensities in individual cells was exported from Flowjo as scale values, combined, and analysed using the 'monocle' R package available on BioConductor. A cellDataSet was created with 'gaussianff()' as the family function parameter. Typically, monocle defaults to a negative binomial. However, the data used is not RNA-seq data and is already normalised, thus the 'gaussianff()' parameter is used. Dimensionality reduction was done to a maximum of 2 components utilising the 'DDRTree' method. After which, cells were ordered to obtain a pseudotime trajectory and were also categorised by monocle into three different 'states'. This trajectory was then plotted, with a smooth line fitted along the trajectory. Cells were also colored according to disease state category. Average expression values for each marker were also plotted.

Boxplots shown in this manuscript were generated using Graphpad Prism 7 software. Heatmaps and visual UMAP plots were generated using custom R-scripts.

ELISPOT

Enzyme-linked immunosorbent spot (ELISPOT) assays for the detection of IFN-g-producing cells in the presence of dengue peptides were performed as described previously (Rivino et al., 2013). Briefly, an equal number of thawed PBMCs (80-100 x 10^5 cells) were incubated overnight in

human IFN-g capture antibody-coated 96 wells with or without peptide mixtures (1 mg/mL) or with PMA/ionomycin (PMA 2 ng/mL; Iono 1 mg/mL) as a positive control. DMSO concentration for the peptide mixtures did not exceed 0.5 % in each well. Spots were counted using an automated ELISPOT reader (Immunospot; Cellular Technology Limited). The number of IFN-γ-producing cells was expressed as spot-forming cells (SFC) relative to 1 x 10^5 PBMCs. Values were calculated by subtracting the number of spots detected in the nonstimulated control wells. Values were considered positive if they were equal or greater than 5 spots and at least 2 times above the means of the unstimulated control wells.

Luminex

Plasma from 49 patients and 4 controls was diluted 1:2 with PBS and probed with the Immune Monitoring 65-Plex Human ProcartaPlex Panel (Invitrogen) and Human Luminex Performance Assay Base Kit, MMP Panel (R & D systems). Samples or standards were incubated with fluorescent-coded magnetic beads, which had been pre-coated with respective capture antibodies. After an overnight incubation at 4°C with shaking, plates were washed twice with wash buffer. Biotinylated detection antibodies were incubated with the complex for 30 mins and subsequently Streptavidin-PE was added and incubated for another 30 mins. Plates were washed twice again, and beads were re-suspended with sheath fluid before acquiring on the FLEXMAP® 3D (Luminex). Data acquisition was done using xPONENT® 4.0 (Luminex) acquisition software and data analysis was done using Bio-Plex Manager™ 6.1.1 (Bio-Rad). Standard curves were generated with a 5-parameter logistic algorithm. Cytokine concentrations were transformed with $\log_{10}$ transformation prior to analysis.

To generate PCA analysis, only cytokines for which there were n ≥30 results within the range of accurate detection were selected for analysis. Any out of range values for these 46 cytokines were substituted with the minimum or maximum detected values of the respective analyte.

Abbreviations: BLC, B lymphocyte chemoattractant; HGF, hepatocyte growth factor; I-TAC, Interferon-inducible T cell alpha chemoattractant; IP-10, IFN-γ-induced protein 10; LIF, leukemia inhibitory factor; MCP-1, monocyte chemoattractant protein 1; MIG, monokine induced by IFN-γ; TNF-RII, Tumor necrosis factor receptor 2.

Statistical Analyses

Changes in cell frequencies over time were determined by the Kruskal-Wallis test, followed by Dunn's Post-hoc test. For changes in $\log_{10}$ cytokine concentrations, one-way ANOVA was applied, followed by Tukey's Post-hoc test. p-values were corrected with the Benjamini-Hochberg (BH) method. For visual clarity, boxplot figures only show parameters where Dunn's post-hoc test or Tukey's Post-hoc test resulted in BH corrected p-values <0.05 (Table S3, S4). Graph annotations are as follows: * P < 0.05; ** P < 0.01; *** P < 0.001; **** P < 0.0001.

The network analysis combined clinical information, frequencies of cell subsets from mass cytometry analysis, and plasma cytokine measurements (Table S6). To ensure relevance to dengue infection, conditions for inclusion of a parameter were Kruskal-Wallis or ANOVA test results with an uncorrected p-value of <0.05 and minimum unique values ≥ 5. Spearman's correlations, Kruskal Wallis tests, and Fisher exact tests were performed where applicable. Only

results where Spearman's correlations Rho^2 value >0.667, and BH corrected p-values <0.05 were included in the building of the network graph.

Acosta-Rodriguez, E.V., Rivino, L., Geginat, J., Jarrossay, D., Gattorno, M., Lanzavecchia, A., Sallusto, F., and Napolitani, G. (2007). Surface phenotype and antigenic specificity of human interleukin 17–producing T helper memory cells. Nat. Immunol. *8*, 639–646.

Amir, E.D. (2019). Cytometry quality control and reproducibility utilities: ismms-himc/cytutils (Human Immune Monitoring Center at Mount Sinai).

Becht, E., Simoni, Y., Coustan-Smith, E., Maximilien, E., Cheng, Y., Ng, L.G., Campana, D., Newell, E., and Wren, J. (2018). Reverse-engineering flow-cytometry gating strategies for phenotypic labelling and high-performance cell sorting. Bioinformatics.

Cheng, Y., Zhu, Y.O., Becht, E., Aw, P., Chen, J., Poidinger, M., Sessions, P.F. de, Hibberd, M.L., Bertoletti, A., Lim, S.G., et al. (2019). Multifactorial heterogeneity of virus-specific T cells and association with the progression of human chronic hepatitis B infection. Sci. Immunol. *4*, eaau6905.

Finck, R., Simonds, E.F., Jager, A., Krishnaswamy, S., Sachs, K., Fantl, W., Pe'er, D., Nolan, G.P., and Bendall, S.C. (2013). Normalization of mass cytometry data with bead standards. Cytom. Part J. Int. Soc. Anal. Cytol. *83*, 483–494.

Gosselin, A., Monteiro, P., Chomont, N., Diaz-Griffero, F., Said, E.A., Fonseca, S., Wacleche, V., El-Far, M., Boulassel, M.-R., Routy, J.-P., et al. (2010). Peripheral Blood CCR4+CCR6+ and CXCR3+CCR6+ CD4+ T Cells Are Highly Permissive to HIV-1 Infection. J. Immunol. *184*, 1604–1616.

Kunicki, M.A., Hernandez, L.C.A., Davis, K.L., Bacchetta, R., and Roncarolo, M.-G. (2017). Identity and Diversity of Human Peripheral Th and T Regulatory Cells Defined by Single-Cell Mass Cytometry. J. Immunol. ji1701025.

Leong, M.L., and Newell, E.W. (2015). Multiplexed Peptide-MHC Tetramer Staining with Mass Cytometry. Methods Mol. Biol. Clifton NJ *1346*, 115–131.

Levine, J.H., Simonds, E.F., Bendall, S.C., Davis, K.L., Amir, E.D., Tadmor, M.D., Litvin, O., Fienberg, H.G., Jager, A., Zunder, E.R., et al. (2015). Data-Driven Phenotypic Dissection of AML Reveals Progenitor-like Cells that Correlate with Prognosis. Cell *162*, 184–197.

McInnes, L., and Healy, J. (2018). UMAP: Uniform Manifold Approximation and Projection for Dimension Reduction. ArXiv180203426 Cs Stat.

Newell, E.W., Sigal, N., Nair, N., Kidd, B.A., Greenberg, H.B., and Davis, M.M. (2013). Combinatorial tetramer staining and mass cytometry analysis facilitate T-cell epitope mapping and characterization. Nat. Biotechnol. *31*, 623–629.

Qiu, X., Mao, Q., Tang, Y., Wang, L., Chawla, R., Pliner, H.A., and Trapnell, C. (2017). Reversed graph embedding resolves complex single-cell trajectories. Nat. Methods *14*, 979.

Rivino, L., Kumaran, E.A.P., Jovanovic, V., Nadua, K., Teo, E.W., Pang, S.W., Teo, G.H., Gan, V.C.H., Lye, D.C., Leo, Y.S., et al. (2013). Differential Targeting of Viral Components by CD4+ versus CD8+ T Lymphocytes in Dengue Virus Infection. J. Virol. *87*, 2693–2706.

Vita, R., Mahajan, S., Overton, J.A., Dhanda, S.K., Martini, S., Cantrell, J.R., Wheeler, D.K., Sette, A., and Peters, B. (2018). The Immune Epitope Database (IEDB): 2018 update. Nucleic Acids Res.

Weiskopf, D., Bangs, D.J., Sidney, J., Kolla, R.V., Silva, A.D.D., Silva, A.M. de, Crotty, S., Peters, B., and Sette, A. (2015). Dengue virus infection elicits highly polarized CX3CR1+ cytotoxic CD4+ T cells associated with protective immunity. Proc. Natl. Acad. Sci. *112*, E4256–E4263.

Wong, M.T., Chen, J., Narayanan, S., Lin, W., Anicete, R., Kiaang, H.T.K., De Lafaille, M.A.C., Poidinger, M., and Newell, E.W. (2015). Mapping the Diversity of Follicular Helper T Cells in Human Blood and Tonsils Using High-Dimensional Mass Cytometry Analysis. Cell Rep. *11*, 1822–1833.

MATERIALS AND METHODS

Patients and ethics statement

All patients in the Mab cohort (Table S1) were recruited at Tan Tock Seng Hospital in Singapore during acute dengue infection and blood samples were taken after informed consent at three time points of infection: acute, post-febrile, and early convalescent (days 6-9, 14-21 and 40-80 from fever onset, respectively). Patients were diagnosed by a team of clinicians according to WHO guidelines, as described previously (Rivino et al., 2013). The study was conducted in accordance with the Declaration of Helsinki and approved by the Singapore National Healthcare Group ethical review board (DSRB 2008/00293). Blood from anonymous healthy donors were also collected at the Singapore Immunology Network (SIgN) with approval by the Centralised Institutional Review Board (CIRB 2017/2806). Blood samples were collected in EDTA vacutainer tubes. PBMCs were isolated from peripheral blood by Ficoll gradient purification and cryopreserved in 90% fetal calf serum + 10% DMSO.

All methods for patients in the LNA cohort were identical except for the time points of blood sample collection: acute (days 3-8 from fever onset), post-febrile (days 10-27), late convalescent (days 173-192), and late (days 357-381). The Singapore National Healthcare Group ethical review board number is NHG DSRB 2015/00528.

Antibody and streptavidin labelling

Recombinant streptavidin was expressed and refolded in house as previously described (Cheng et al., 2019; Newell et al., 2013). Purified antibodies without carrier proteins were purchased as

listed in Table S2. Maleimide-conjugated DN3 MAXPAR chelating polymers (Fluidigm) were loaded with heavy metal isotopes (Fluidigm) according to the manufacturer's recommendations. For antibody conjugations, 100 µg of purified antibodies lacking carrier proteins were coupled with the metal polymer structures according to the protocol provided by Fluidigm. For streptavidin conjugations, 100 µg of streptavidin was conjugated to the respective metal-loaded DN3 polymer and finally diluted to a concentration of 200 µg/mL for subsequent tetramerization (Leong and Newell, 2015; Newell et al., 2013).

Virus epitope selection and prediction

DENV and control epitopes for HLA-B*58:01, A*11:01, and A*24:02 were obtained from the IEDB (Vita et al., 2018) and previous papers (Rivino et al., 2013). Serotype variations to cover all 4 DENV serotypes were predicted for these peptides. In addition, 9- and 10-mer peptides based on the sequence of DENV-1 virus (strain TSV08-1-I) and DENV-2 virus (strain TSV01-2) were predicted for their binding affinity to A*11:01 and A*24:02 using the consensus prediction tool on the IEDB website (Vita et al., 2018). For each allele, peptides were selected if they were in the top 0.8% of binders. All peptides were synthesized by Mimotopes (Australia) with purity > 80%.

Peptides sequence similarity and cluster assignment

To avoid incorrect interpretations from cross-reactive T cell epitopes, sequences were loaded onto a Biostrings-based R-written environment (Newell et al., 2013). The biological sequence and matching algorithm performed pairwise alignment to calculate the peptide binding score based

on their sequence similarity and HLA anchor point. Peptides with similar binding scores were assigned the same peptide cluster number. The resulting peptide cluster assignations are listed in Table S2. Peptides within the same cluster were then assigned the same triple SAV-metal codings.

UV peptide exchange to generate pHLA

UV-cleavable peptide HLA monomers were produced in-house as previously described (Cheng et al., 2019; Newell et al., 2013). Peptide exchange was performed at 100 µg/mL of HLA monomer in 100 µL PBS with 25 µM of peptide of interest in a 96-well plate. The mixture was exposed to 365 nm UV irradiation for 2 sessions of 5 minutes using a UVP CL-1000 Ultraviolet Crosslinker, and then stored at 4°C overnight to complete the exchange.

84-plex or 220-plex combinatorial pHLA tetramer production

Each metal-labelled streptavidin was diluted to 25 µg/mL in EDTA-free W buffer. To eliminate false positives from non-specific tetramer staining, two different configurations of triple streptavidin-metal codings were generated. The metal-labeled streptavidins were mixed using an automated liquid distribution robot (TECAN Freedom Evo200). On the day of cell staining, the triple streptavidin-metal mixtures were added to the corresponding pHLA in a stepwise manner of three additions, with 10 min of incubation time at room temperature between each step. Finally, 10 µM D-biotin (Sigma) was added to the tetramerized pHLA complexes to saturate unbound streptavidin. All tetramers for each configuration were combined and concentrated

down to 5 µg/mL per pHLA tetramer in 10% FBS CyFACS buffer using an Amicon Ultra 50 kDa filter (Millipore).

Cell Staining and Mass Cytometry Acquisition

All antibody and tetramer cocktails were prepared on the day of cell staining. Antibodies used for pre-staining (Table S2) were combined in a 30 kDa filter (Amicon Ultra, Millipore), washed and centrifuged with PBS twice to remove azide content. Before staining, all tetramer and antibody cocktails were filtered using a 0.1 µM filter (Ultrafree, Millipore) to remove aggregates. Cryopreserved cells were thawed and washed twice with complete RPMI media (10% FBS, 1% penicillin/streptomycin/L-glutamine) (Gibco, Invitrogen). 80% of the cells were split evenly into two wells for Panel 1 staining with two different tetramer configurations and the remaining 20% of cells were used for staining with Panel 2. Cells were incubated with 50 nM dasatinib and pre-stain antibodies in complete RPMI for 30 min at 37°C. After pre-staining, cells were washed in cold CyFACS buffer (PBS with 4% FCS, 2 mM EDTA, and 0.05% Azide) and incubated on ice with 200 nM Cisplatin (Sigma) for 5 min. Cells were then washed twice with CyFACs and incubated for 1 hour at room temperature with tetramer cocktail. Subsequently, cells were washed and stained with primary surface antibodies and/or EasySep Human T cell Isolation Cocktail (STEMCELL) for 15 min at 4°C. Cells were washed and stained with secondary surface antibodies and/or EasySep Dextran RapidSpheres (STEMCELL) for 15 min at 4°C.

For intracellular and intranuclear antibody staining, cells were washed and fixed with Foxp3/Transcription Factor Fix/Perm buffer (eBiosciences) for 30 min on ice. Cells were then

washed with 1X Permeabilization buffer (eBiosciences) and stained with primary intracellular antibodies for 30 min on ice, washed twice, followed by incubation with secondary intracellular antibodies for 30 min on ice. Finally, cells were washed with 1X Permeabilization buffer and fixed in 2% PFA (paraformaldehyde, Electron Microscopy Science) at 4°C overnight.

On the next day, PFA was removed and cells were incubated with cellular barcodes for 30 min on ice as previously described (Wong et al., 2015). Cells were then washed first with perm buffer, followed by CyFACS. Cellular DNA was labeled at room temperature with 250 nM iridium interchelator (Fluidigm) diluted in 2% PFA for 20 min. Subsequently, cells were washed with CyFACS, combined and enriched for CD3+ T cells using a magnet (EasySep). Immediately before mass cytometry acquisition, cells were washed twice with MilliQ water and passed into a filter top FACS tube. 1.5% of Four EQ beads (Fluidigm DVS) were mixed with the cell suspension. The first two batches of samples were acquired on a CyTOF2 instrument and the third batch of samples was acquired on a Helios instrument.

Mass Cytometry Data Pre-Processing

After mass cytometry acquisition, the signal of each parameter was normalized based on the equilibration beads added to each sample (Finck et al., 2013). All zero values were randomized by an R-script that uniformly distributes values between minus-one and zero. Individual samples were debarcoded manually in FlowJo v10 (Treestar, Inc.). For identification of tetramer positive CD8 cells, live singlet CD8+ T cells were gated and exported individually as CD8 Config 1 and CD8 Config 2 fcs files. Thresholds for each metal-labelled streptavidin channel were manually defined

by gating a CD8+ T cell population that was negative for all of the streptavidin channels and using that as the tetramer negative baseline. Using the tetramer deconvolution algorithm (Newell et al., 2013), only cells positive for above-threshold staining in only three streptavidin channels were considered positive for tetramer staining. Frequencies of tetramer positive cells identified in the two different tetramer coding configurations of the same donor were further calculated for their likely correspondence using statistical stimulation, with $p<0.1$ being considered as plausible detection. Lastly, where there were multiple time points from the same donor, if the concordance in frequency of tetramer+ T cells failed to be achieved at two or more time points, the hit was removed.

High Dimensional Cytometric Data Visualization and Analysis

All data were transformed in R using the "logicleTransform" function by using the "flowCore" package (parameters: w = 0.25, t = 16,409, m = 4.5, a = 0). UMAP dimensionality reduction analysis was carried out using the R package uwot (McInnes and Healy, 2018)(Becht et al., in press). Louvain clustering analyses using Phenograph was used to identify clusters based on marker expression in an automated unbiased fashion (Levine et al., 2015). These clusters were then curated and named according to definitions that have previously been reported in the literature (Acosta-Rodriguez et al., 2007; Gosselin et al., 2010; Kunicki et al., 2017; Weiskopf et al., 2015; Wong et al., 2015). Hypergate was used to identify optimized gating strategies that accurately described these subsets using as few markers as possible (Becht et al., 2018). For this study, optimized gating strategies mostly selected for combinations of surface chemokine receptors, not transcription factors. For simplicity of presentation, we have not appended "-like"

to subsets defined by surface markers. The optimized gating strategies were then applied to the different batches of experiments, with manual changes to account for batch effects, and from there frequencies of the various populations and subsets were identified. The code for calculating Jensen Shannon Distances was adapted from the R package cytutils (Amir, 2019)

For Monocle 2 analysis (Qiu et al., 2017), the dataset of marker intensities in individual cells was exported from Flowjo as scale values, combined, and analysed using the 'monocle' R package available on BioConductor. A cellDataSet was created with 'gaussianff()' as the family function parameter. Typically, monocle defaults to a negative binomial. However, the data used is not RNA-seq data and is already normalised, thus the 'gaussianff()' parameter is used. Dimensionality reduction was done to a maximum of 2 components utilising the 'DDRTree' method. After which, cells were ordered to obtain a pseudotime trajectory and were also categorised by monocle into three different 'states'. This trajectory was then plotted, with a smooth line fitted along the trajectory. Cells were also colored according to disease state category. Average expression values for each marker were also plotted.

Boxplots shown in this manuscript were generated using Graphpad Prism 7 software. Heatmaps and visual UMAP plots were generated using custom R-scripts.

ELISPOT

Enzyme-linked immunosorbent spot (ELISPOT) assays for the detection of IFN-g-producing cells in the presence of dengue peptides were performed as described previously (Rivino et al., 2013). Briefly, an equal number of thawed PBMCs (80-100 x 10^5 cells) were incubated overnight in

human IFN-g capture antibody-coated 96 wells with or without peptide mixtures (1 mg/mL) or with PMA/ionomycin (PMA 2 ng/mL; Iono 1 mg/mL) as a positive control. DMSO concentration for the peptide mixtures did not exceed 0.5 % in each well. Spots were counted using an automated ELISPOT reader (Immunospot; Cellular Technology Limited). The number of IFN-γ-producing cells was expressed as spot-forming cells (SFC) relative to 1 x 10^5 PBMCs. Values were calculated by subtracting the number of spots detected in the nonstimulated control wells. Values were considered positive if they were equal or greater than 5 spots and at least 2 times above the means of the unstimulated control wells.

Luminex

Plasma from 49 patients and 4 controls was diluted 1:2 with PBS and probed with the Immune Monitoring 65-Plex Human ProcartaPlex Panel (Invitrogen) and Human Luminex Performance Assay Base Kit, MMP Panel (R & D systems). Samples or standards were incubated with fluorescent-coded magnetic beads, which had been pre-coated with respective capture antibodies. After an overnight incubation at 4°C with shaking, plates were washed twice with wash buffer. Biotinylated detection antibodies were incubated with the complex for 30 mins and subsequently Streptavidin-PE was added and incubated for another 30 mins. Plates were washed twice again, and beads were re-suspended with sheath fluid before acquiring on the FLEXMAP® 3D (Luminex). Data acquisition was done using xPONENT® 4.0 (Luminex) acquisition software and data analysis was done using Bio-Plex Manager™ 6.1.1 (Bio-Rad). Standard curves were generated with a 5-parameter logistic algorithm. Cytokine concentrations were transformed with $\log_{10}$ transformation prior to analysis.

To generate PCA analysis, only cytokines for which there were n ≥30 results within the range of accurate detection were selected for analysis. Any out of range values for these 46 cytokines were substituted with the minimum or maximum detected values of the respective analyte.

Abbreviations: BLC, B lymphocyte chemoattractant; HGF, hepatocyte growth factor; I-TAC, Interferon-inducible T cell alpha chemoattractant; IP-10, IFN-γ-induced protein 10; LIF, leukemia inhibitory factor; MCP-1, monocyte chemoattractant protein 1; MIG, monokine induced by IFN-γ; TNF-RII, Tumor necrosis factor receptor 2.

Statistical Analyses

Changes in cell frequencies over time were determined by the Kruskal-Wallis test, followed by Dunn's Post-hoc test. For changes in $\log_{10}$ cytokine concentrations, one-way ANOVA was applied, followed by Tukey's Post-hoc test. p-values were corrected with the Benjamini-Hochberg (BH) method. For visual clarity, boxplot figures only show parameters where Dunn's post-hoc test or Tukey's Post-hoc test resulted in BH corrected p-values <0.05 (Table S3, S4). Graph annotations are as follows: * P < 0.05; ** P < 0.01; *** P < 0.001; **** P < 0.0001.

The network analysis combined clinical information, frequencies of cell subsets from mass cytometry analysis, and plasma cytokine measurements (Table S6). To ensure relevance to dengue infection, conditions for inclusion of a parameter were Kruskal-Wallis or ANOVA test results with an uncorrected p-value of <0.05 and minimum unique values ≥ 5. Spearman's correlations, Kruskal Wallis tests, and Fisher exact tests were performed where applicable. Only

results where Spearman's correlations Rho^2 value >0.667, and BH corrected p-values <0.05 were included in the building of the network graph.

Acosta-Rodriguez, E.V., Rivino, L., Geginat, J., Jarrossay, D., Gattorno, M., Lanzavecchia, A., Sallusto, F., and Napolitani, G. (2007). Surface phenotype and antigenic specificity of human interleukin 17–producing T helper memory cells. Nat. Immunol. *8*, 639–646.

Amir, E.D. (2019). Cytometry quality control and reproducibility utilities: ismms-himc/cytutils (Human Immune Monitoring Center at Mount Sinai).

Becht, E., Simoni, Y., Coustan-Smith, E., Maximilien, E., Cheng, Y., Ng, L.G., Campana, D., Newell, E., and Wren, J. (2018). Reverse-engineering flow-cytometry gating strategies for phenotypic labelling and high-performance cell sorting. Bioinformatics.

Cheng, Y., Zhu, Y.O., Becht, E., Aw, P., Chen, J., Poidinger, M., Sessions, P.F. de, Hibberd, M.L., Bertoletti, A., Lim, S.G., et al. (2019). Multifactorial heterogeneity of virus-specific T cells and association with the progression of human chronic hepatitis B infection. Sci. Immunol. *4*, eaau6905.

Finck, R., Simonds, E.F., Jager, A., Krishnaswamy, S., Sachs, K., Fantl, W., Pe'er, D., Nolan, G.P., and Bendall, S.C. (2013). Normalization of mass cytometry data with bead standards. Cytom. Part J. Int. Soc. Anal. Cytol. *83*, 483–494.

Gosselin, A., Monteiro, P., Chomont, N., Diaz-Griffero, F., Said, E.A., Fonseca, S., Wacleche, V., El-Far, M., Boulassel, M.-R., Routy, J.-P., et al. (2010). Peripheral Blood CCR4+CCR6+ and CXCR3+CCR6+ CD4+ T Cells Are Highly Permissive to HIV-1 Infection. J. Immunol. *184*, 1604–1616.

Kunicki, M.A., Hernandez, L.C.A., Davis, K.L., Bacchetta, R., and Roncarolo, M.-G. (2017). Identity and Diversity of Human Peripheral Th and T Regulatory Cells Defined by Single-Cell Mass Cytometry. J. Immunol. ji1701025.

Leong, M.L., and Newell, E.W. (2015). Multiplexed Peptide-MHC Tetramer Staining with Mass Cytometry. Methods Mol. Biol. Clifton NJ *1346*, 115–131.

Levine, J.H., Simonds, E.F., Bendall, S.C., Davis, K.L., Amir, E.D., Tadmor, M.D., Litvin, O., Fienberg, H.G., Jager, A., Zunder, E.R., et al. (2015). Data-Driven Phenotypic Dissection of AML Reveals Progenitor-like Cells that Correlate with Prognosis. Cell *162*, 184–197.

McInnes, L., and Healy, J. (2018). UMAP: Uniform Manifold Approximation and Projection for Dimension Reduction. ArXiv180203426 Cs Stat.

Newell, E.W., Sigal, N., Nair, N., Kidd, B.A., Greenberg, H.B., and Davis, M.M. (2013). Combinatorial tetramer staining and mass cytometry analysis facilitate T-cell epitope mapping and characterization. Nat. Biotechnol. *31*, 623–629.

Qiu, X., Mao, Q., Tang, Y., Wang, L., Chawla, R., Pliner, H.A., and Trapnell, C. (2017). Reversed graph embedding resolves complex single-cell trajectories. Nat. Methods *14*, 979.

Rivino, L., Kumaran, E.A.P., Jovanovic, V., Nadua, K., Teo, E.W., Pang, S.W., Teo, G.H., Gan, V.C.H., Lye, D.C., Leo, Y.S., et al. (2013). Differential Targeting of Viral Components by CD4+ versus CD8+ T Lymphocytes in Dengue Virus Infection. J. Virol. *87*, 2693–2706.

Vita, R., Mahajan, S., Overton, J.A., Dhanda, S.K., Martini, S., Cantrell, J.R., Wheeler, D.K., Sette, A., and Peters, B. (2018). The Immune Epitope Database (IEDB): 2018 update. Nucleic Acids Res.

Weiskopf, D., Bangs, D.J., Sidney, J., Kolla, R.V., Silva, A.D.D., Silva, A.M. de, Crotty, S., Peters, B., and Sette, A. (2015). Dengue virus infection elicits highly polarized CX3CR1+ cytotoxic CD4+ T cells associated with protective immunity. Proc. Natl. Acad. Sci. *112*, E4256–E4263.

Wong, M.T., Chen, J., Narayanan, S., Lin, W., Anicete, R., Kiaang, H.T.K., De Lafaille, M.A.C., Poidinger, M., and Newell, E.W. (2015). Mapping the Diversity of Follicular Helper T Cells in Human Blood and Tonsils Using High-Dimensional Mass Cytometry Analysis. Cell Rep. *11*, 1822–1833.

Fig 1

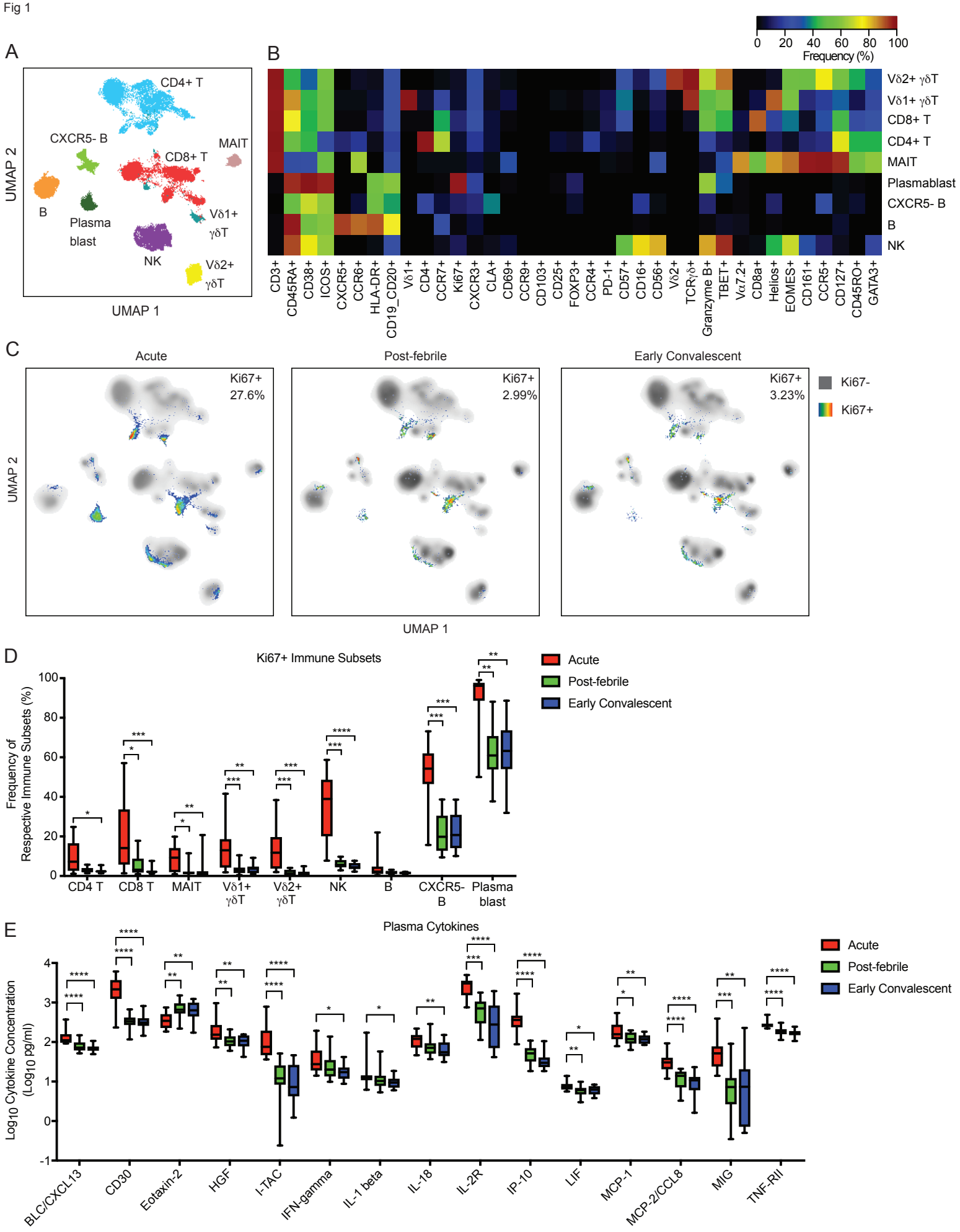
A
CD4+ T
CXCR5- B
MAIT
CD8+ T
B
Plasma blast
Vδ1+ γδT
NK
Vδ2+ γδT
UMAP 2
UMAP 1
B
0 20 40 60 80 100
Frequency (%)
Vδ2+ γδT
Vδ1+ γδT
CD8+ T
CD4+ T
MAIT
Plasmablast
CXCR5- B
B
NK
CD3+ CD45RA+ CD38+ ICOS+ CXCR5+ CCR6+ HLA-DR+ CD19_CD20+ Vδ1+ CD4+ CCR7+ Ki67+ CXCR3+ CLA+ CD69+ CCR9+ CD103+ CD25+ FOXP3+ CCR4+ PD-1+ CD57+ CD16+ CD56+ Vδ2+ TCRγδ+ Granzyme B+ TBET+ Vα7.2+ CD8a+ Helios+ EOMES+ CD161+ CCR5+ CD127+ CD45RO+ GATA3+
C
Acute
Post-febrile
Early Convalescent
Ki67+ 27.6%
Ki67+ 2.99%
Ki67+ 3.23%
Ki67-
Ki67+
UMAP 2
UMAP 1
D
Ki67+ Immune Subsets
Frequency of Respective Immune Subsets (%)
Acute
Post-febrile
Early Convalescent
CD4 T
CD8 T
MAIT
Vδ1+ γδT
Vδ2+ γδT
NK
B
CXCR5- B
Plasma blast
E
Plasma Cytokines
Log10 Cytokine Concentration (Log10 pg/ml)
Acute
Post-febrile
Early Convalescent
BLC/CXCL13
CD30
Eotaxin-2
HGF
I-TAC
IFN-gamma
IL-1 beta
IL-18
IL-2R
IP-10
LIF
MCP-1
MCP-2/CCL8
MIG
TNF-RII

Fig 2

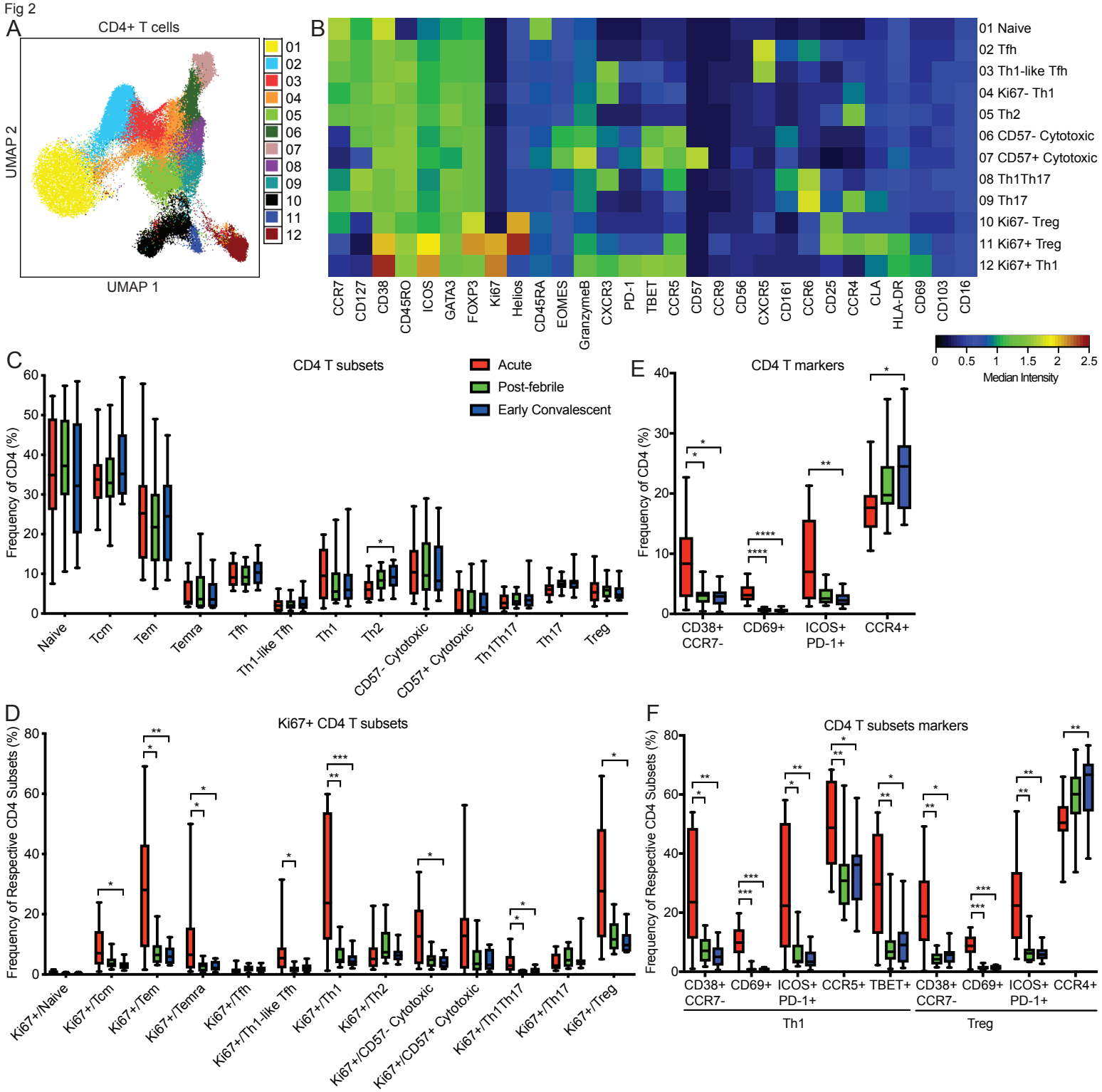
A
CD4+ T cells
UMAP 2
UMAP 1
01
02
03
04
05
06
07
08
09
10
11
12
B
01 Naive
02 Tfh
03 Th1-like Tfh
04 Ki67- Th1
05 Th2
06 CD57- Cytotoxic
07 CD57+ Cytotoxic
08 Th1Th17
09 Th17
10 Ki67- Treg
11 Ki67+ Treg
12 Ki67+ Th1
CCR7
CD127
CD38
CD45RO
ICOS
GATA3
FOXP3
Ki67
Helios
CD45RA
EOMES
GranzymeB
CXCR3
PD-1
TBET
CCR5
CD57
CCR9
CD56
CXCR5
CD161
CCR6
CD25
CCR4
CLA
HLA-DR
CD69
CD103
CD16
0
0.5
1
1.5
2
2.5
Median Intensity
C
CD4 T subsets
Acute
Post-febrile
Early Convalescent
Frequency of CD4 (%)
Naive
Tcm
Tem
Temra
Tfh
Th1-like Tfh
Th1
Th2
CD57- Cytotoxic
CD57+ Cytotoxic
Th1Th17
Th17
Treg
E
CD4 T markers
Frequency of CD4 (%)
CD38+ CCR7-
CD69+
ICOS+ PD-1+
CCR4+
D
Ki67+ CD4 T subsets
Frequency of Respective CD4 Subsets (%)
Ki67+/Naive
Ki67+/Tcm
Ki67+/Tem
Ki67+/Temra
Ki67+/Tfh
Ki67+/Th1-like Tfh
Ki67+/Th1
Ki67+/Th2
Ki67+/CD57- Cytotoxic
Ki67+/CD57+ Cytotoxic
Ki67+/Th1Th17
Ki67+/Th17
Ki67+/Treg
F
CD4 T subsets markers
Frequency of Respective CD4 Subsets (%)
CD38+ CCR7-
CD69+
ICOS+ PD-1+
CCR5+
TBET+
CD38+ CCR7-
CD69+
ICOS+ PD-1+
CCR4+
Th1
Treg

Fig 3

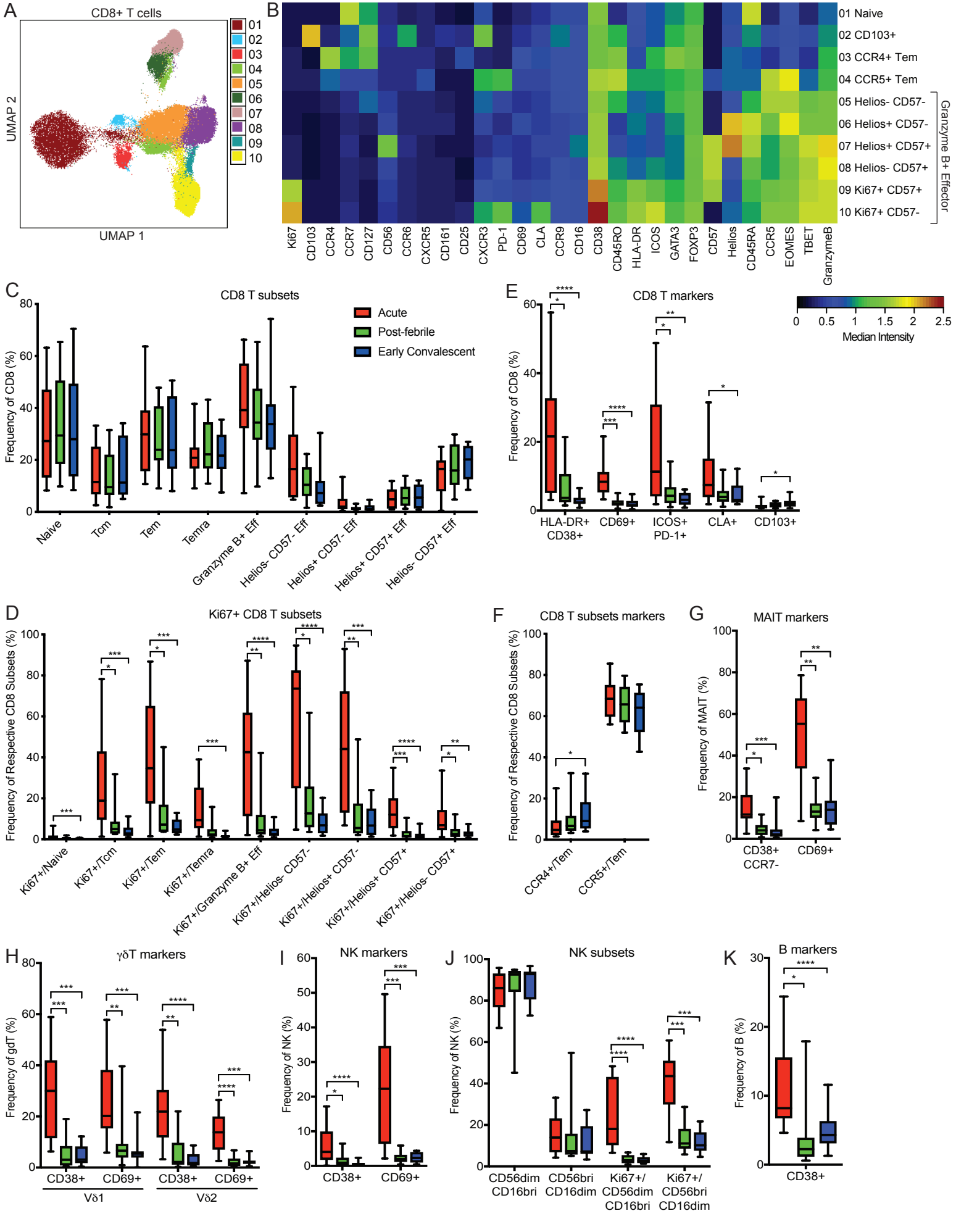
A
CD8+ T cells
UMAP 2
UMAP 1
01
02
03
04
05
06
07
08
09
10
B
01 Naive
02 CD103+
03 CCR4+ Tem
04 CCR5+ Tem
05 Helios- CD57-
06 Helios+ CD57-
07 Helios+ CD57+
08 Helios- CD57+
09 Ki67+ CD57+
10 Ki67+ CD57-
Granzyme B+ Effector
Ki67
CD103
CCR4
CCR7
CD127
CD56
CCR6
CXCR5
CD161
CD25
CXCR3
PD-1
CD69
CLA
CCR9
CD16
CD38
CD45RO
HLA-DR
ICOS
GATA3
FOXP3
CD57
Helios
CD45RA
CCR5
EOMES
TBET
GranzymeB
C
CD8 T subsets
Acute
Post-febrile
Early Convalescent
Frequency of CD8 (%)
Naive
Tcm
Tem
Temra
Granzyme B+ Eff
Helios- CD57- Eff
Helios+ CD57- Eff
Helios+ CD57+ Eff
Helios- CD57+ Eff
E
CD8 T markers
Median Intensity
Frequency of CD8 (%)
HLA-DR+ CD38+
CD69+
ICOS+ PD-1+
CLA+
CD103+
D
Ki67+ CD8 T subsets
Frequency of Respective CD8 Subsets (%)
Ki67+/Naive
Ki67+/Tcm
Ki67+/Tem
Ki67+/Temra
Ki67+/Granzyme B+ Eff
Ki67+/Helios- CD57-
Ki67+/Helios+ CD57-
Ki67+/Helios+ CD57+
Ki67+/Helios- CD57+
F
CD8 T subsets markers
Frequency of Respective CD8 Subsets (%)
CCR4+/Tem
CCR5+/Tem
G
MAIT markers
Frequency of MAIT (%)
CD38+ CCR7-
CD69+
H
γδT markers
Frequency of gdT (%)
CD38+
CD69+
CD38+
CD69+
Vδ1
Vδ2
I
NK markers
Frequency of NK (%)
CD38+
CD69+
J
NK subsets
Frequency of NK (%)
CD56dim CD16bri
CD56bri CD16dim
Ki67+/ CD56dim CD16bri
Ki67+/ CD56bri CD16dim
K
B markers
Frequency of B (%)
CD38+

Fig 4

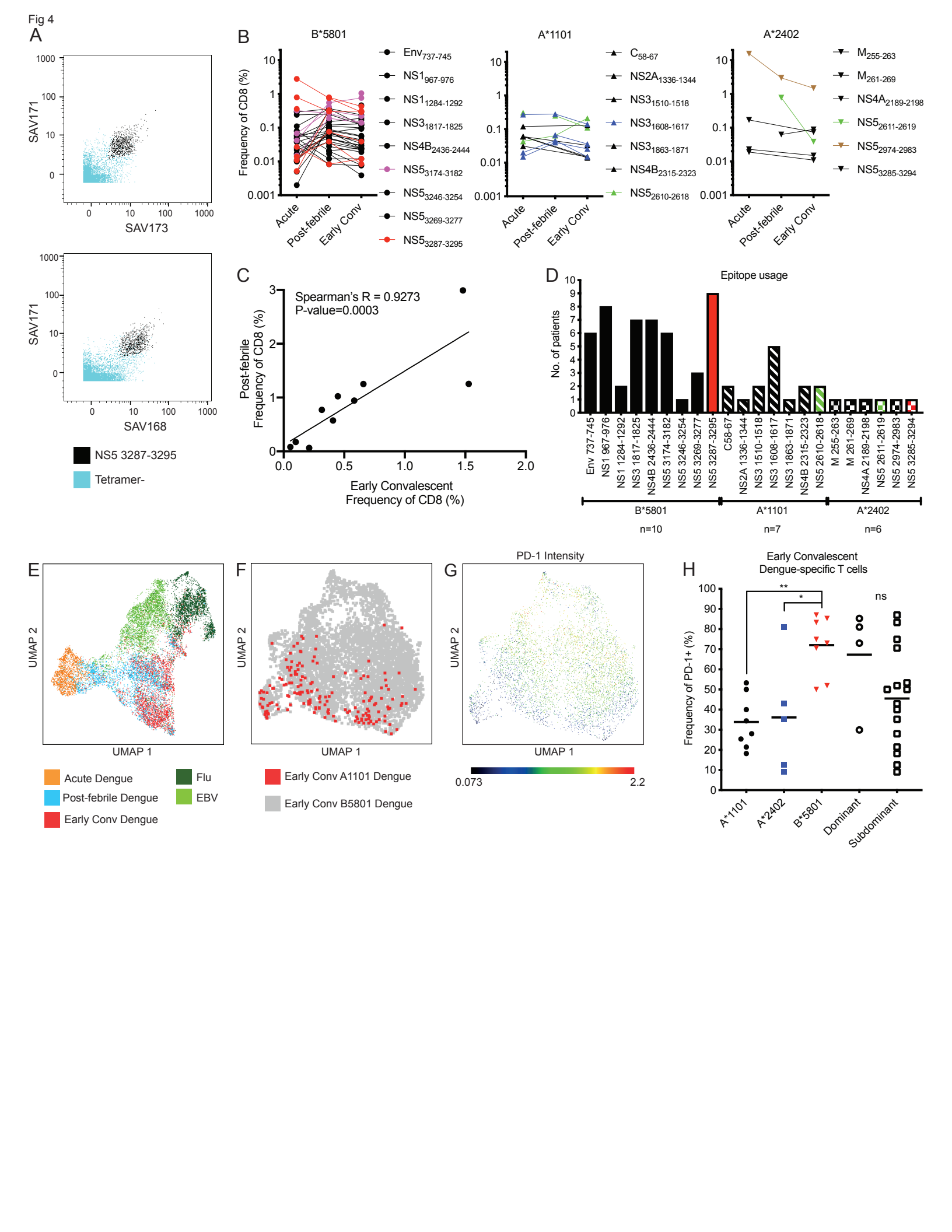
A
SAV171
SAV173
SAV168
NS5 3287-3295
Tetramer-
B
B*5801
A*1101
A*2402
Frequency of CD8 (%)
Acute
Post-febrile
Early Conv
Env737-745
NS1967-976
NS11284-1292
NS31817-1825
NS4B2436-2444
NS53174-3182
NS53246-3254
NS53269-3277
NS53287-3295
C58-67
NS2A1336-1344
NS31510-1518
NS31608-1617
NS31863-1871
NS4B2315-2323
NS52610-2618
M255-263
M261-269
NS4A2189-2198
NS52611-2619
NS52974-2983
NS53285-3294
C
Spearman's R = 0.9273
P-value=0.0003
Post-febrile Frequency of CD8 (%)
Early Convalescent Frequency of CD8 (%)
D
Epitope usage
No. of patients
Env 737-745
NS1 967-976
NS1 1284-1292
NS3 1817-1825
NS4B 2436-2444
NS5 3174-3182
NS5 3246-3254
NS5 3269-3277
NS5 3287-3295
C58-67
NS2A 1336-1344
NS3 1510-1518
NS3 1608-1617
NS3 1863-1871
NS4B 2315-2323
NS5 2610-2618
M 255-263
M 261-269
NS4A 2189-2198
NS5 2611-2619
NS5 2974-2983
NS5 3285-3294
B*5801
A*1101
A*2402
n=10
n=7
n=6
E
UMAP 2
UMAP 1
Acute Dengue
Post-febrile Dengue
Early Conv Dengue
Flu
EBV
F
UMAP 2
UMAP 1
Early Conv A1101 Dengue
Early Conv B5801 Dengue
G
PD-1 Intensity
UMAP 2
UMAP 1
0.073
2.2
H
Early Convalescent
Dengue-specific T cells
Frequency of PD-1+ (%)
**
*
ns
A*1101
A*2402
B*5801
Dominant
Subdominant

Fig 5

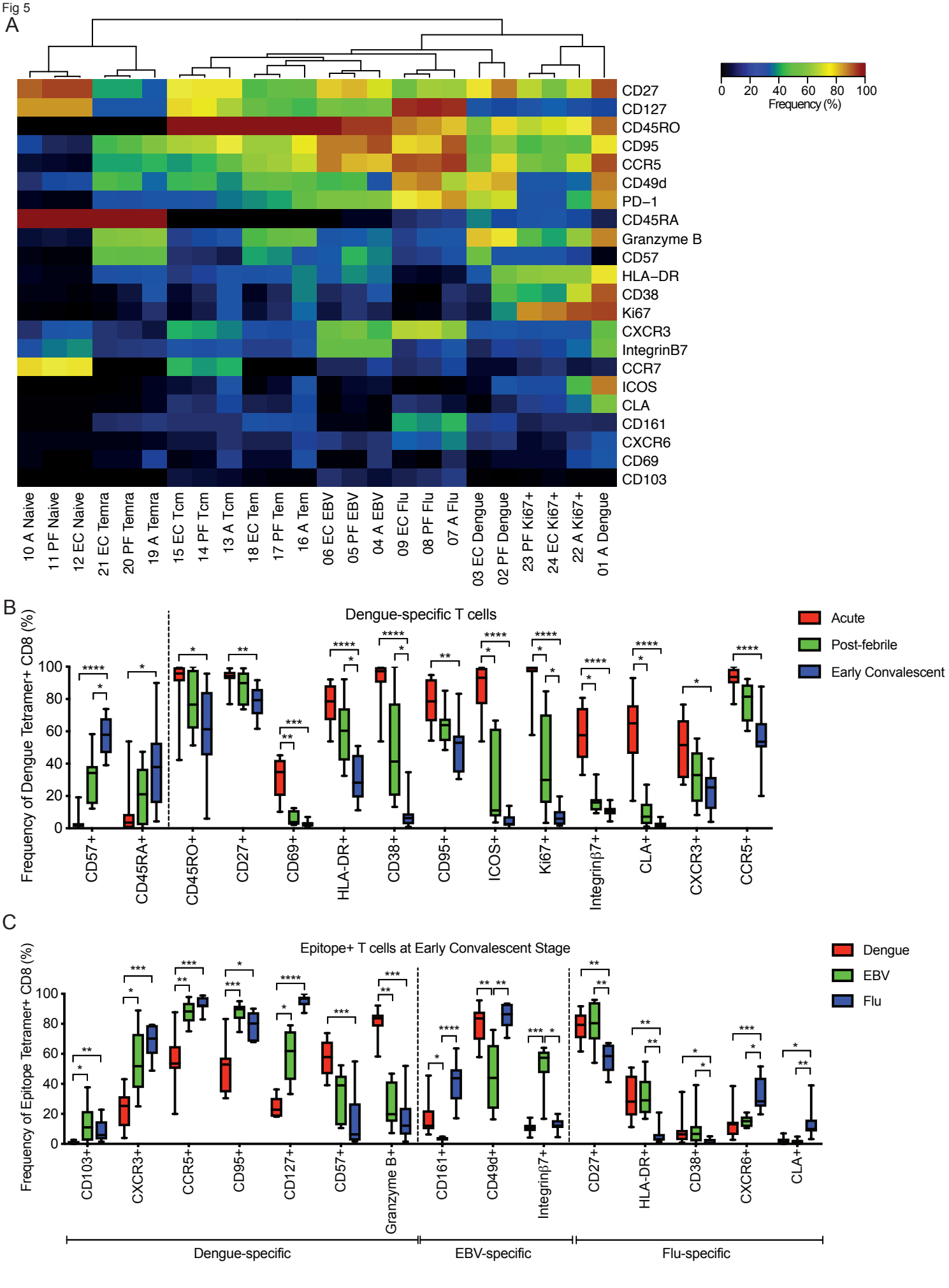
A
CD27
CD127
CD45RO
CD95
CCR5
CD49d
PD−1
CD45RA
Granzyme B
CD57
HLA−DR
CD38
Ki67
CXCR3
IntegrinB7
CCR7
ICOS
CLA
CD161
CXCR6
CD69
CD103
0 20 40 60 80 100
Frequency (%)
10 A Naive
11 PF Naive
12 EC Naive
21 EC Temra
20 PF Temra
19 A Temra
15 EC Tcm
14 PF Tcm
13 A Tcm
18 EC Tem
17 PF Tem
16 A Tem
06 EC EBV
05 PF EBV
04 A EBV
09 EC Flu
08 PF Flu
07 A Flu
03 EC Dengue
02 PF Dengue
23 PF Ki67+
24 EC Ki67+
22 A Ki67+
01 A Dengue
B
Dengue-specific T cells
Frequency of Dengue Tetramer+ CD8 (%)
Acute
Post-febrile
Early Convalescent
CD57+
CD45RA+
CD45RO+
CD27+
CD69+
HLA-DR+
CD38+
CD95+
ICOS+
Ki67+
Integrinβ7+
CLA+
CXCR3+
CCR5+
C
Epitope+ T cells at Early Convalescent Stage
Frequency of Epitope Tetramer+ CD8 (%)
Dengue
EBV
Flu
CD103+
CXCR3+
CCR5+
CD95+
CD127+
CD57+
Granzyme B+
CD161+
CD49d+
Integrinβ7+
CD27+
HLA-DR+
CD38+
CXCR6+
CLA+
Dengue-specific
EBV-specific
Flu-specific

Fig 6

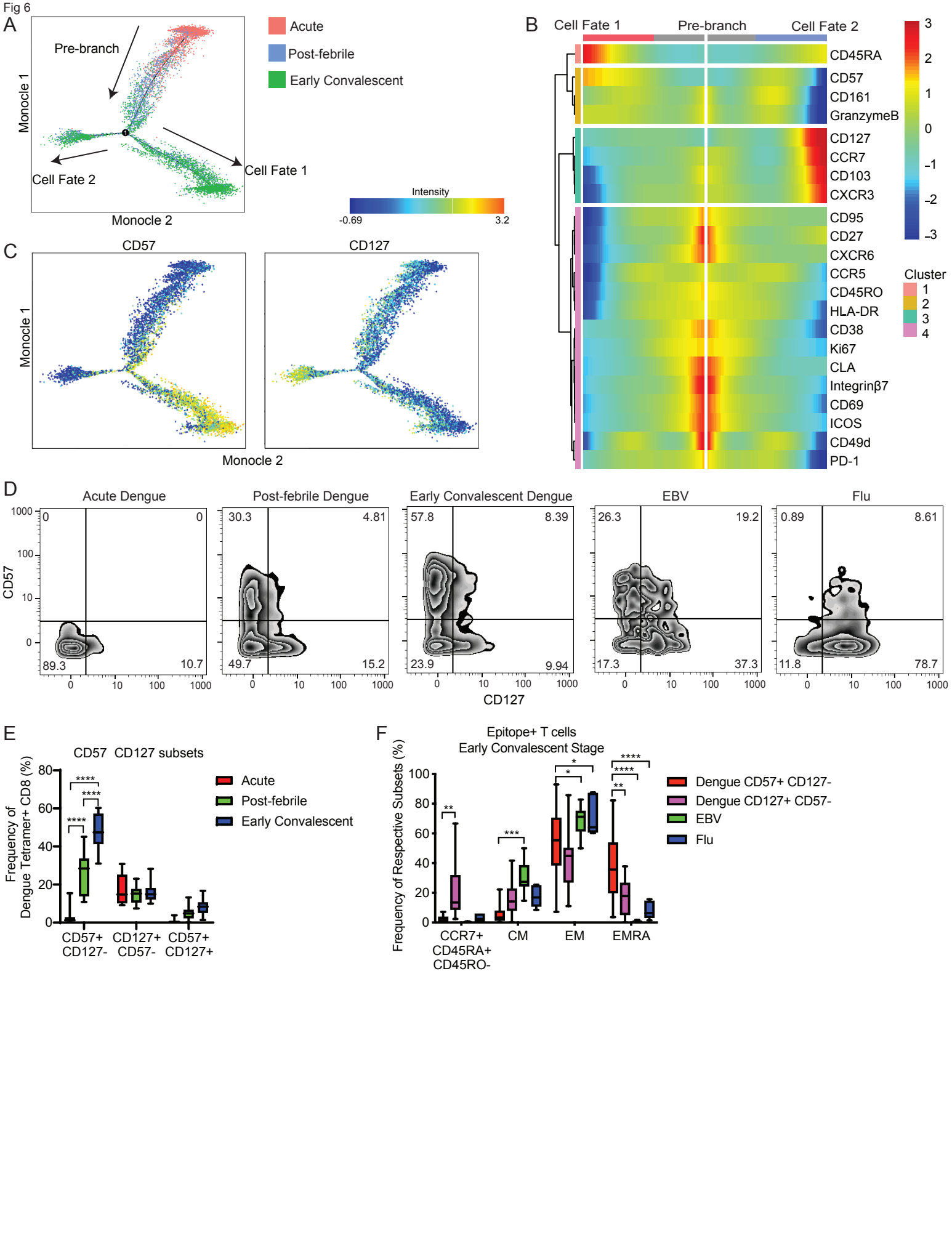
A
Pre-branch
Monocle 1
Cell Fate 2
Cell Fate 1
Monocle 2
Acute
Post-febrile
Early Convalescent
Intensity
-0.69
3.2
B
Cell Fate 1
Pre-branch
Cell Fate 2
CD45RA
CD57
CD161
GranzymeB
CD127
CCR7
CD103
CXCR3
CD95
CD27
CXCR6
CCR5
CD45RO
HLA-DR
CD38
Ki67
CLA
Integrinβ7
CD69
ICOS
CD49d
PD-1
3
2
1
0
-1
-2
-3
Cluster
1
2
3
4
C
CD57
CD127
Monocle 1
Monocle 2
D
Acute Dengue
Post-febrile Dengue
Early Convalescent Dengue
EBV
Flu
CD57
CD127
0
0
89.3
10.7
30.3
4.81
49.7
15.2
57.8
8.39
23.9
9.94
26.3
19.2
17.3
37.3
0.89
8.61
11.8
78.7
1000
100
10
0
E
CD57 CD127 subsets
Frequency of Dengue Tetramer+ CD8 (%)
Acute
Post-febrile
Early Convalescent
CD57+ CD127-
CD127+ CD57-
CD57+ CD127+
F
Epitope+ T cells
Early Convalescent Stage
Frequency of Respective Subsets (%)
Dengue CD57+ CD127-
Dengue CD127+ CD57-
EBV
Flu
CCR7+ CD45RA+ CD45RO-
CM
EM
EMRA

Fig 7

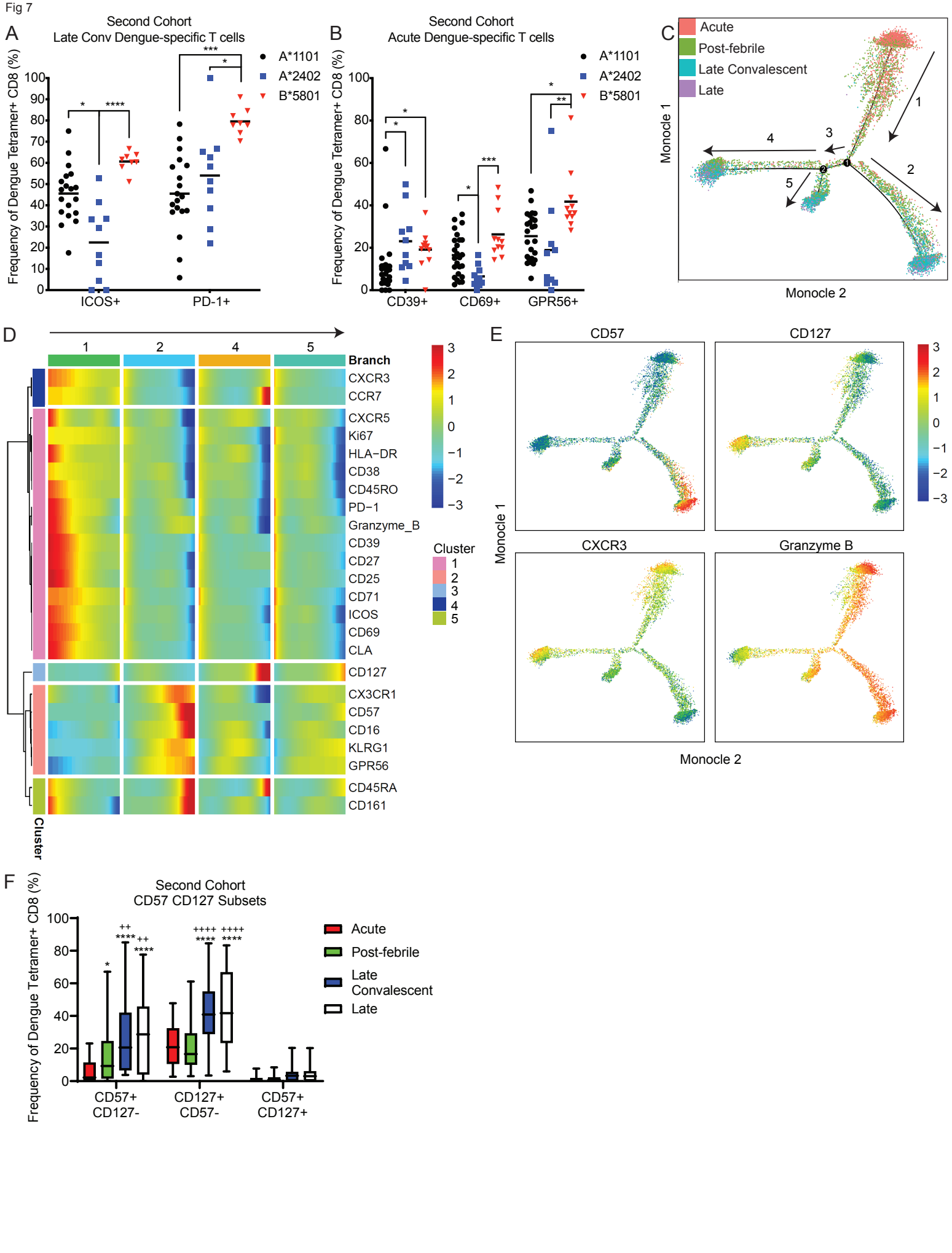
A
Second Cohort
Late Conv Dengue-specific T cells
Frequency of Dengue Tetramer+ CD8 (%)
A*1101
A*2402
B*5801
ICOS+
PD-1+
B
Second Cohort
Acute Dengue-specific T cells
CD39+
CD69+
GPR56+
C
Acute
Post-febrile
Late Convalescent
Late
Monocle 1
Monocle 2
D
Branch
Cluster
CXCR3
CCR7
CXCR5
Ki67
HLA−DR
CD38
CD45RO
PD−1
Granzyme_B
CD39
CD27
CD25
CD71
ICOS
CD69
CLA
CD127
CX3CR1
CD57
CD16
KLRG1
GPR56
CD45RA
CD161
E
CD57
CD127
CXCR3
Granzyme B
Monocle 1
Monocle 2
F
Second Cohort
CD57 CD127 Subsets
Frequency of Dengue Tetramer+ CD8 (%)
CD57+ CD127-
CD127+ CD57-
CD57+ CD127+
Acute
Post-febrile
Late Convalescent
Late

Figure S1

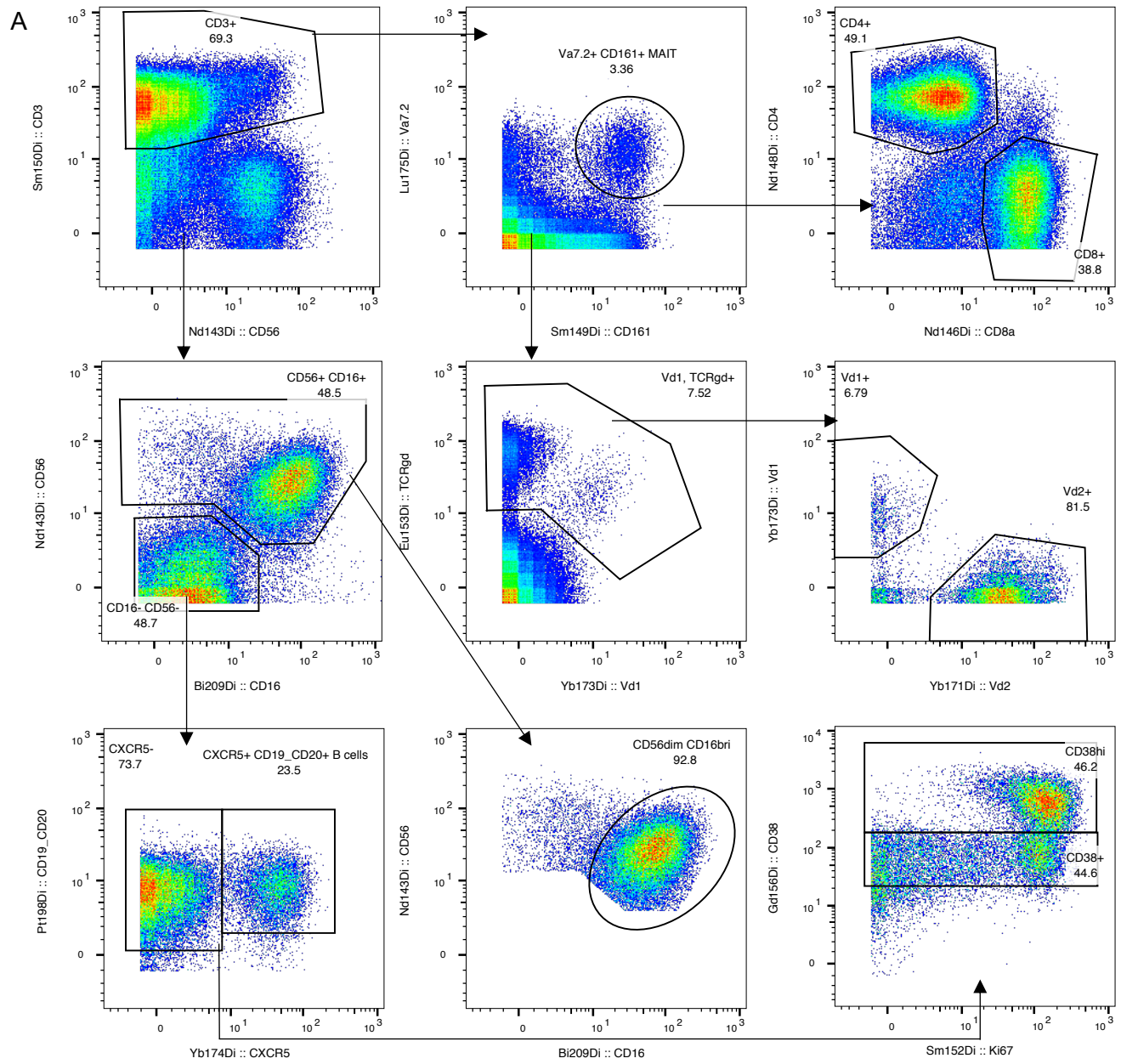
A
CD3+
69.3
Sm150Di :: CD3
Nd143Di :: CD56
Va7.2+ CD161+ MAIT
3.36
Lu175Di :: Va7.2
Sm149Di :: CD161
CD4+
49.1
Nd148Di :: CD4
CD8+
38.8
Nd146Di :: CD8a
CD56+ CD16+
48.5
Nd143Di :: CD56
CD16- CD56-
48.7
Bi209Di :: CD16
Vd1, TCRgd+
7.52
Eu153Di :: TCRgd
Yb173Di :: Vd1
Vd1+
6.79
Yb173Di :: Vd1
Vd2+
81.5
Yb171Di :: Vd2
CXCR5-
73.7
CXCR5+ CD19_CD20+ B cells
23.5
Pt198Di :: CD19_CD20
Yb174Di :: CXCR5
CD56dim CD16bri
92.8
Nd143Di :: CD56
Bi209Di :: CD16
CD38hi
46.2
CD38+
44.6
Gd156Di :: CD38
Sm152Di :: Ki67

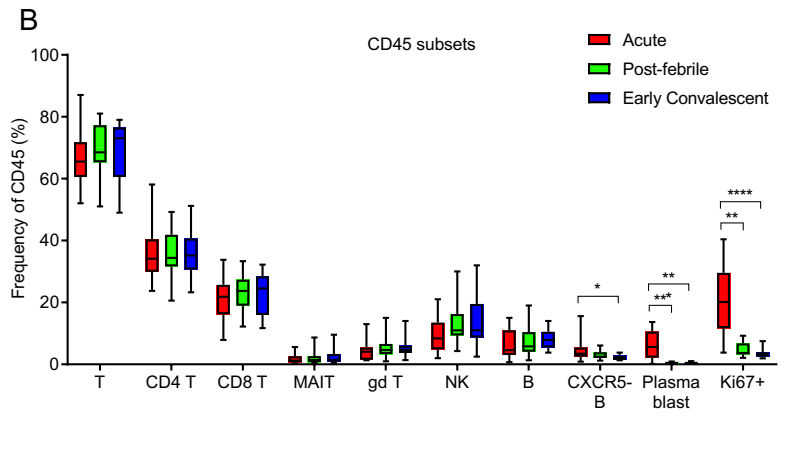
B
CD45 subsets
Acute
Post-febrile
Early Convalescent
Frequency of CD45 (%)
T
CD4 T
CD8 T
MAIT
gd T
NK
B
CXCR5- B
Plasma blast
Ki67+

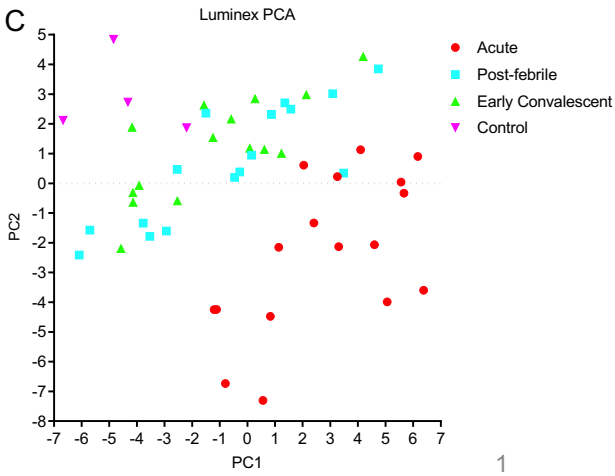
C
Luminex PCA
Acute
Post-febrile
Early Convalescent
Control
PC2
PC1

Figure S2

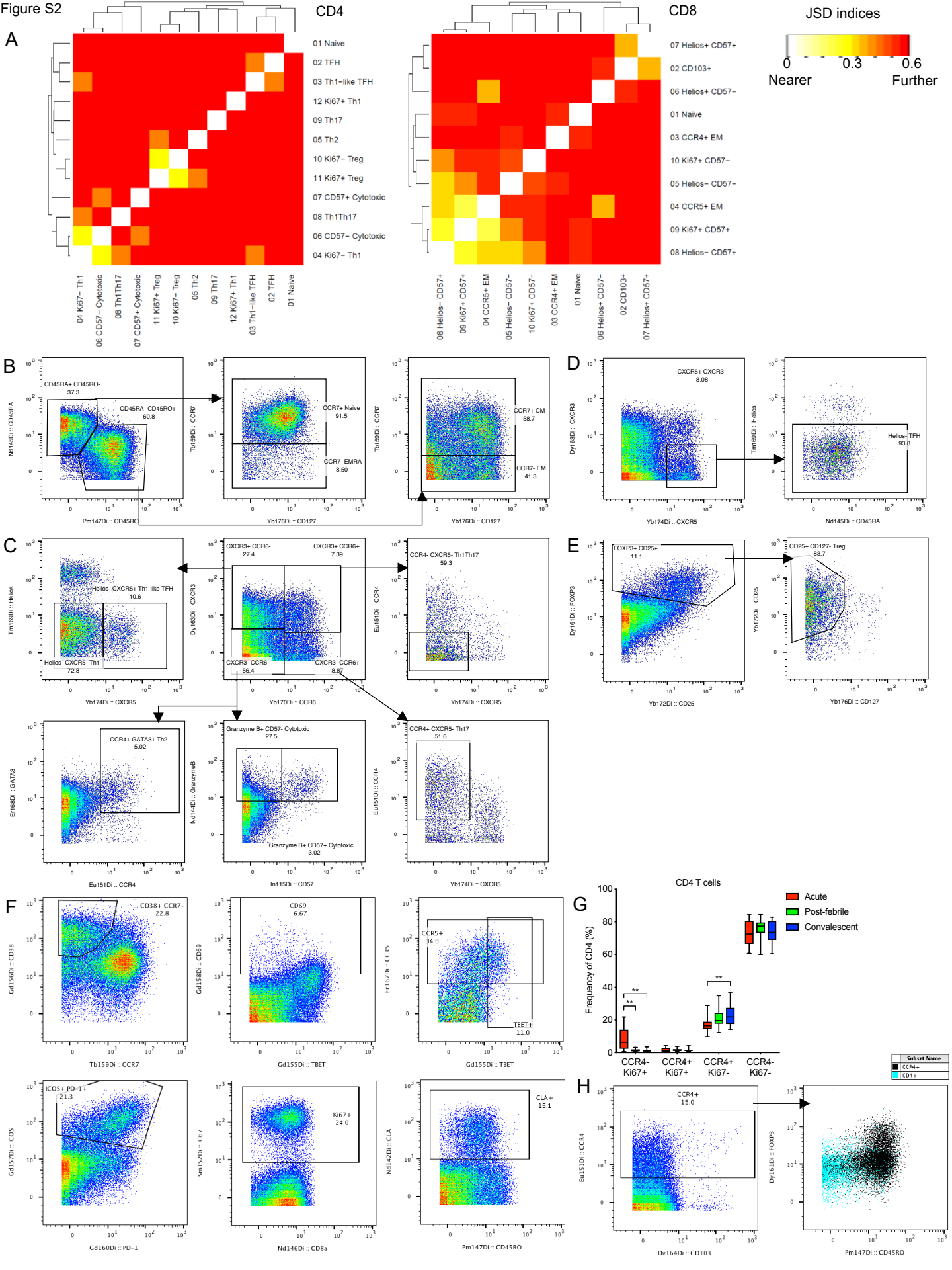
A
CD4
01 Naive
02 TFH
03 Th1−like TFH
12 Ki67+ Th1
09 Th17
05 Th2
10 Ki67− Treg
11 Ki67+ Treg
07 CD57+ Cytotoxic
08 Th1Th17
06 CD57− Cytotoxic
04 Ki67− Th1
04 Ki67− Th1
06 CD57− Cytotoxic
08 Th1Th17
07 CD57+ Cytotoxic
11 Ki67+ Treg
10 Ki67− Treg
05 Th2
09 Th17
12 Ki67+ Th1
03 Th1−like TFH
02 TFH
01 Naive
CD8
07 Helios+ CD57+
02 CD103+
06 Helios+ CD57−
01 Naive
03 CCR4+ EM
10 Ki67+ CD57−
05 Helios− CD57−
04 CCR5+ EM
09 Ki67+ CD57+
08 Helios− CD57+
08 Helios− CD57+
09 Ki67+ CD57+
04 CCR5+ EM
05 Helios− CD57−
10 Ki67+ CD57−
03 CCR4+ EM
01 Naive
06 Helios+ CD57−
02 CD103+
07 Helios+ CD57+
JSD indices
0
0.3
0.6
Nearer
Further
B
CD45RA+ CD45RO− 37.3
CD45RA− CD45RO+ 60.8
Nd145Di :: CD45RA
Pm147Di :: CD45RO
CCR7+ Naive 91.5
CCR7− EMRA 8.50
Tb159Di :: CCR7
Yb176Di :: CD127
CCR7+ CM 58.7
CCR7− EM 41.3
D
CXCR5+ CXCR3− 8.08
Dy163Di :: CXCR3
Yb174Di :: CXCR5
Tm169Di :: Helios
Helios− TFH 93.8
Nd145Di :: CD45RA
C
Helios− CXCR5+ Th1−like TFH 10.6
Helios− CXCR5− Th1 72.8
Tm169Di :: Helios
Yb174Di :: CXCR5
CXCR3+ CCR6− 27.4
CXCR3+ CCR6+ 7.39
CXCR3− CCR6− 56.4
CXCR3− CCR6+ 8.87
Dy165Di :: CXCR3
Yb170Di :: CCR6
CCR4− CXCR5− Th1Th17 59.3
Eu151Di :: CCR4
Yb174Di :: CXCR5
E
FOXP3+ CD25+ 11.1
Dy161Di :: FOXP3
Yb172Di :: CD25
CD25+ CD127− Treg 83.7
Yb172Di :: CD25
Yb176Di :: CD127
CCR4+ GATA3+ Th2 5.02
Er168Di :: GATA3
Eu151Di :: CCR4
Granzyme B+ CD57− Cytotoxic 27.5
Granzyme B+ CD57+ Cytotoxic 3.02
Nd144Di :: GranzymeB
In115Di :: CD57
CCR4+ CXCR5− Th17 51.6
Eu151Di :: CCR4
Yb174Di :: CXCR5
F
CD38+ CCR7− 22.8
Gd156Di :: CD38
Tb159Di :: CCR7
CD69+ 6.67
Gd158Di :: CD69
Gd155Di :: TBET
CCR5+ 34.8
TBET+ 11.0
Er167Di :: CCR5
Gd155Di :: TBET
ICOS+ PD−1+ 21.3
Gd157Di :: ICOS
Gd160Di :: PD−1
Ki67+ 24.8
Sm152Di :: Ki67
Nd146Di :: CD8a
CLA+ 15.1
Nd142Di :: CLA
Pm147Di :: CD45RO
G
CD4 T cells
Frequency of CD4 (%)
100
80
60
40
20
0
**
**
**
CCR4− Ki67+
CCR4+ Ki67+
CCR4+ Ki67−
CCR4− Ki67−
Acute
Post-febrile
Convalescent
H
CCR4+ 15.0
Eu151Di :: CCR4
Dy164Di :: CD103
Dy161Di :: FOXP3
Pm147Di :: CD45RO
Subset Name
CCR4+
CD4+

Figure S3

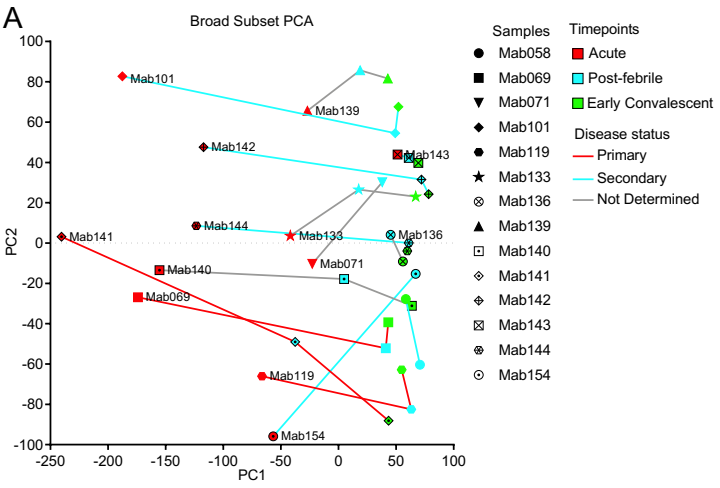
A
Broad Subset PCA
PC1
PC2
Samples
Mab058
Mab069
Mab071
Mab101
Mab119
Mab133
Mab136
Mab139
Mab140
Mab141
Mab142
Mab143
Mab144
Mab154
Timepoints
Acute
Post-febrile
Early Convalescent
Disease status
Primary
Secondary
Not Determined

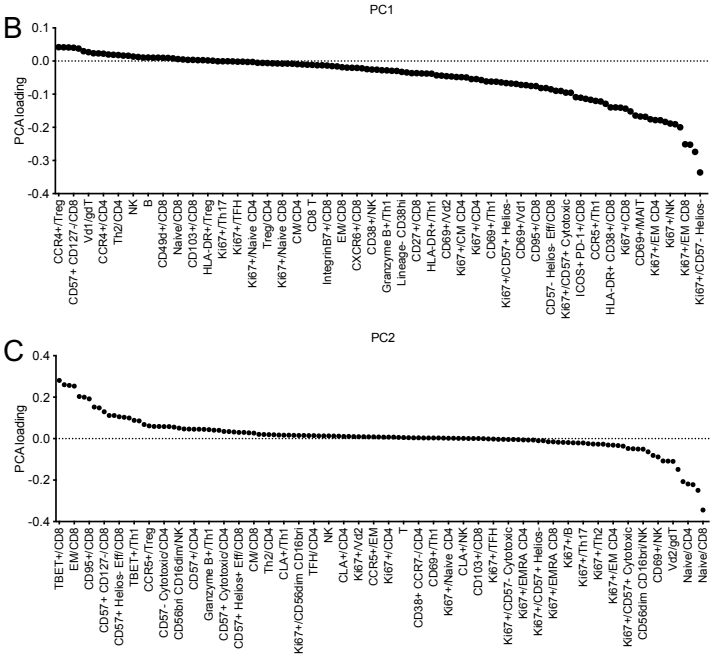
B
PC1
PCA loading
CCR4+/Treg
CD57+ CD127-/CD8
Vd1/gdT
CCR4+/CD4
Th2/CD4
NK
B
CD49d+/CD8
Naive/CD8
CD103+/CD8
HLA-DR+/Treg
Ki67+/Th17
Ki67+/TFH
Ki67+/Naive CD4
Treg/CD4
Ki67+/Naive CD8
CM CD4
CD8 T
Integrin B7+/CD8
EM/CD8
CXCR6+/CD8
CD38+/NK
Granzyme B+/Th1
Lineage- CD38hi
CD27+/CD8
HLA-DR+/Th1
CD69+/Vd2
Ki67+/CM CD4
Ki67+/CD4
CD69+/Th1
Ki67+/CD57+ Helios-
CD95+/Vd1
CD95+/CD8
CD57- Helios+ Eff/CD8
Ki67+/CD57+ Cytotoxic
ICOS+ PD-1+/CD8
CCR5+/Th1
HLA-DR+ CD38+/CD8
Ki67+/CD8
CD69+/MAIT
Ki67+/EM CD4
Ki67+/NK
Ki67+/EM CD8
Ki67+/CD57- Helios-

C
PC2
PCA loading
TBET+/CD8
EM/CD8
CD95+/CD8
CD57+ CD127-/CD8
CD57+ Helios- Eff/CD8
TBET+/Th1
CCR5+/Treg
CD57- Cytotoxic/CD4
CD56bri CD16dim/NK
CD57+/CD4
Granzyme B+/Th1
CD57+ Cytotoxic/CD4
CD57+ Helios+ Eff/CD8
CM/CD8
Th2/CD4
CLA+/Th1
Ki67+/CD56dim CD16bri
TFH/CD4
NK
CLA+/CD4
Ki67+/Vd2
CCR5+/EM
Ki67+/CD4
T
CD38+ CCR7-/CD4
CD69+/Th1
Ki67+/Naive CD4
CLA+/NK
CD103+/CD8
Ki67+/TFH
Ki67+/CD57- Cytotoxic
Ki67+/EMRA CD4
Ki67+/CD57+ Helios-
Ki67+/EMRA CD8
Ki67+/B
Ki67+/Th17
Ki67+/Th2
Ki67+/EM CD4
Ki67+/CD57+ Cytotoxic
CD56dim CD16bri/NK
CD69+/NK
Vd2/gdT
Naive/CD4
Naive/CD8

Figure S4

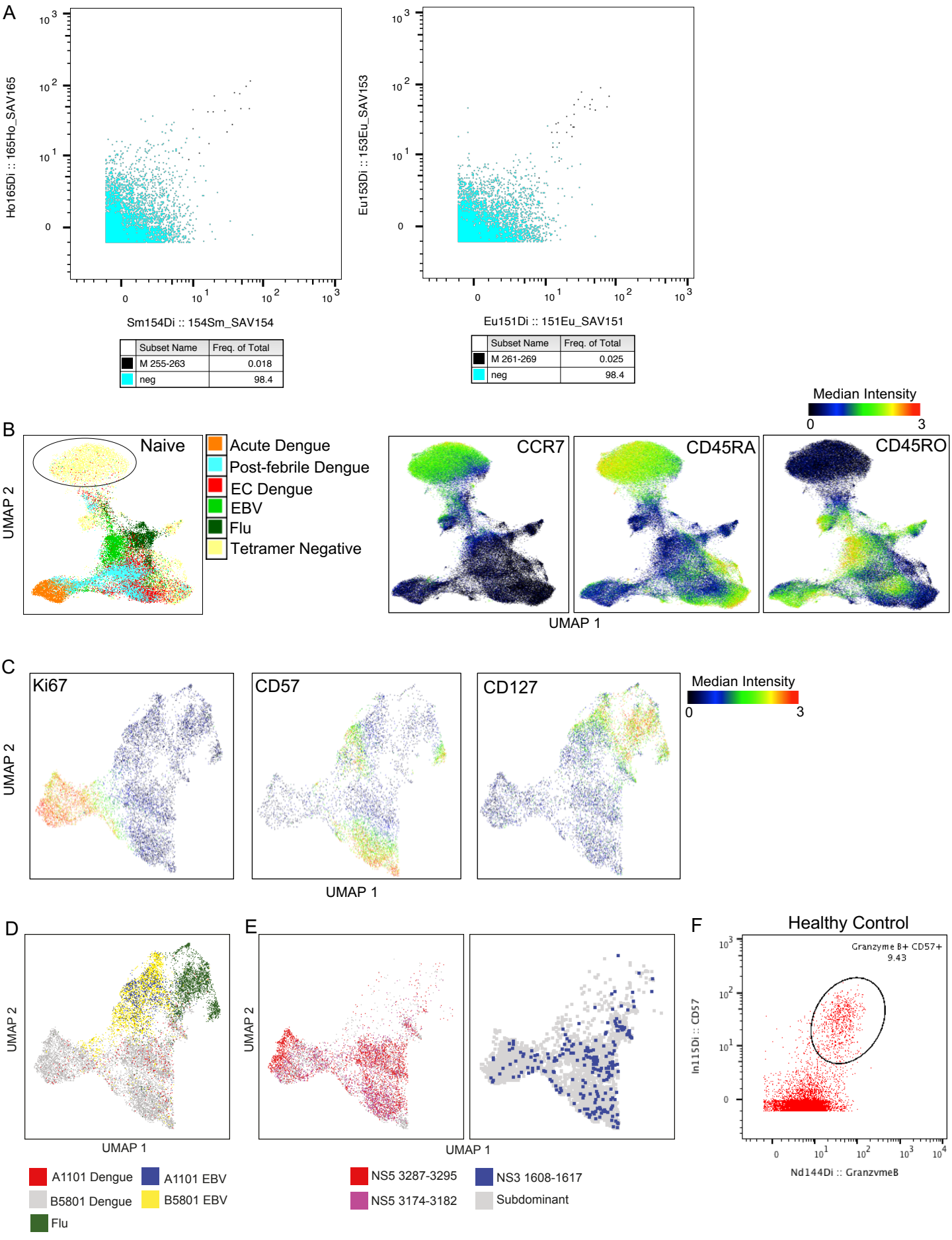
A
Ho165Di :: 165Ho_SAV165
Sm154Di :: 154Sm_SAV154
Subset Name | Freq. of Total
M 255-263 | 0.018
neg | 98.4
Eu153Di :: 153Eu_SAV153
Eu151Di :: 151Eu_SAV151
Subset Name | Freq. of Total
M 261-269 | 0.025
neg | 98.4
B
Median Intensity
0
3
Naive
Acute Dengue
Post-febrile Dengue
EC Dengue
EBV
Flu
Tetramer Negative
CCR7
CD45RA
CD45RO
UMAP 2
UMAP 1
C
Ki67
CD57
CD127
Median Intensity
0
3
UMAP 2
UMAP 1
D
UMAP 2
UMAP 1
A1101 Dengue
A1101 EBV
B5801 Dengue
B5801 EBV
Flu
E
UMAP 2
UMAP 1
NS5 3287-3295
NS3 1608-1617
NS5 3174-3182
Subdominant
F
Healthy Control
Granzyme B+ CD57+
9.43
In115Di :: CD57
Nd144Di :: GranzymeB

Figure S5

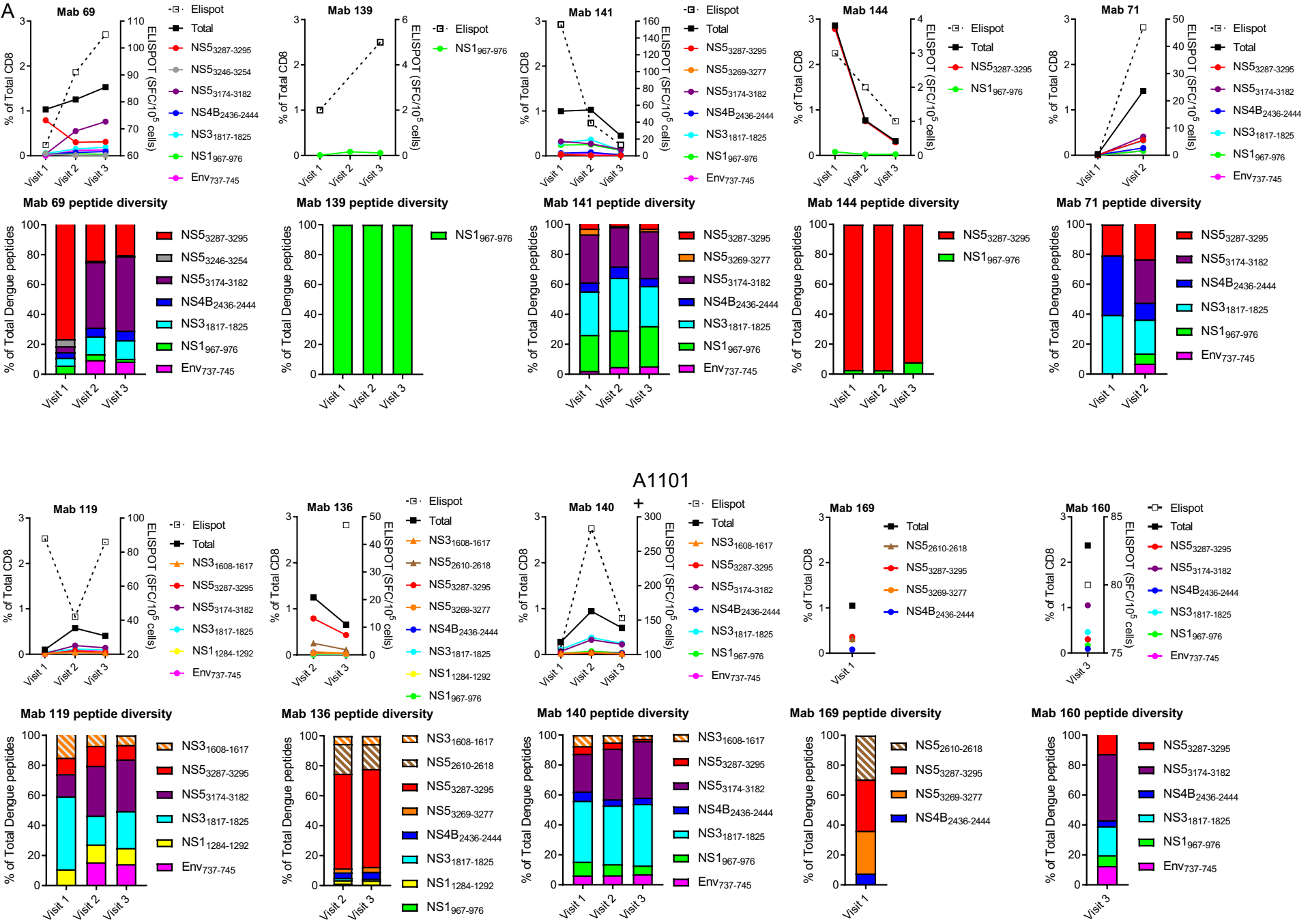
A
Mab 69
Mab 139
Mab 141
Mab 144
Mab 71
% of Total CD8
ELISPOT (SFC/10^5 cells)
Elispot
Total
NS5 3287-3295
NS5 3246-3254
NS5 3269-3277
NS5 3174-3182
NS4B 2436-2444
NS3 1817-1825
NS1 967-976
Env 737-745
Visit 1
Visit 2
Visit 3
Mab 69 peptide diversity
Mab 139 peptide diversity
Mab 141 peptide diversity
Mab 144 peptide diversity
Mab 71 peptide diversity
% of Total Dengue peptides
A1101
Mab 119
Mab 136
Mab 140
Mab 169
Mab 160
NS3 1608-1617
NS5 2610-2618
NS1 1284-1292
Mab 119 peptide diversity
Mab 136 peptide diversity
Mab 140 peptide diversity
Mab 169 peptide diversity
Mab 160 peptide diversity

Figure S5 Continued

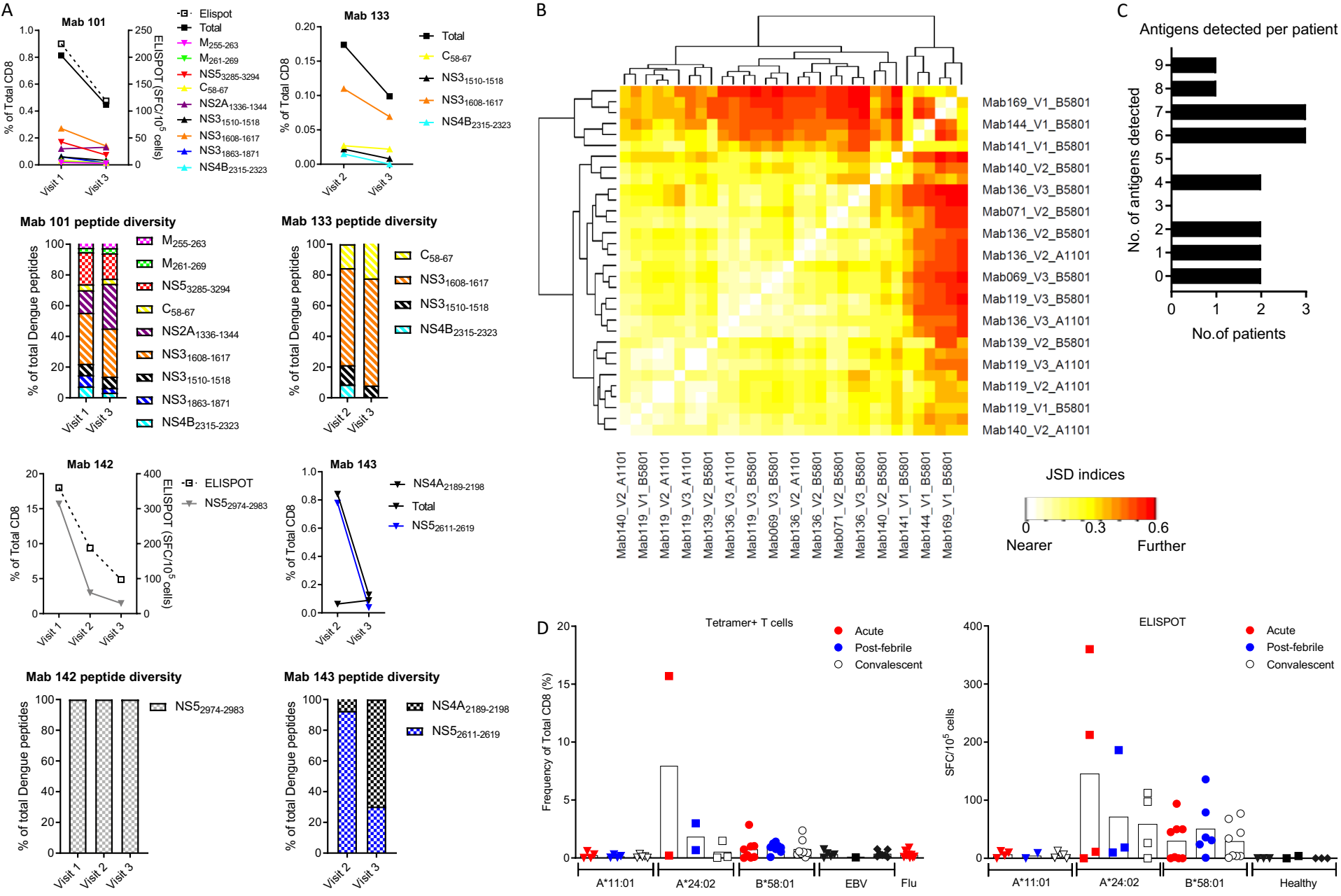

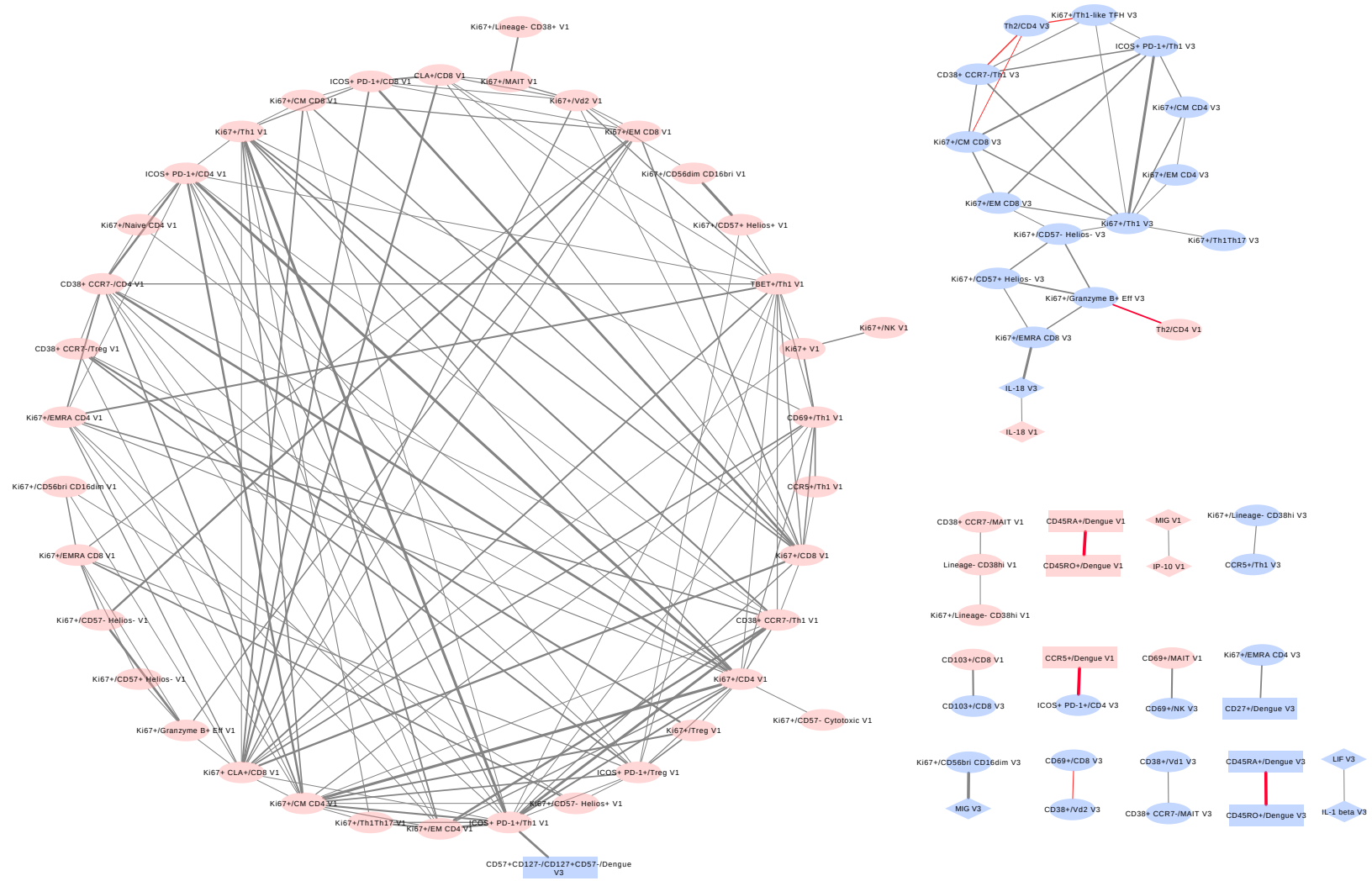
Ki67+/Lineage- CD38+ V1
CLA+/CD8 V1
ICOS+ PD-1+/CD8 V1
Ki67+/MAIT V1
Ki67+/CM CD8 V1
Ki67+/Vd2 V1
Ki67+/Th1 V1
Ki67+/EM CD8 V1
ICOS+ PD-1+/CD4 V1
Ki67+/CD56dim CD16bri V1
Ki67+/Naive CD4 V1
Ki67+/CD57+ Helios+ V1
CD38+ CCR7-/CD4 V1
TBET+/Th1 V1
Ki67+/NK V1
CD38+ CCR7-/Treg V1
Ki67+ V1
Ki67+/EMRA CD4 V1
CD69+/Th1 V1
Ki67+/CD56bri CD16dim V1
CCR5+/Th1 V1
Ki67+/EMRA CD8 V1
Ki67+/CD8 V1
Ki67+/CD57- Helios- V1
CD38+ CCR7-/Th1 V1
Ki67+/CD57+ Helios- V1
Ki67+/CD4 V1
Ki67+/CD57- Cytotoxic V1
Ki67+/Granzyme B+ Eff V1
Ki67+/Treg V1
Ki67+ CLA+/CD8 V1
ICOS+ PD-1+/Treg V1
Ki67+/CM CD4 V1
Ki67+/CD57- Helios+ V1
Ki67+/Th1Th17 V1
ICOS+ PD-1+/Th1 V1
Ki67+/EM CD4 V1
CD57+CD127-/CD127+CD57-/Dengue V3
Ki67+/Th1-like TFH V3
Th2/CD4 V3
ICOS+ PD-1+/Th1 V3
CD38+ CCR7-/Th1 V3
Ki67+/CM CD4 V3
Ki67+/CM CD8 V3
Ki67+/EM CD4 V3
Ki67+/EM CD8 V3
Ki67+/Th1 V3
Ki67+/CD57- Helios- V3
Ki67+/Th1Th17 V3
Ki67+/CD57+ Helios- V3
Ki67+/Granzyme B+ Eff V3
Th2/CD4 V1
Ki67+/EMRA CD8 V3
IL-18 V3
IL-18 V1
CD38+ CCR7-/MAIT V1
CD45RA+/Dengue V1
MIG V1
Ki67+/Lineage- CD38hi V3
Lineage- CD38hi V1
CD45RO+/Dengue V1
IP-10 V1
CCR5+/Th1 V3
Ki67+/Lineage- CD38hi V1
CD103+/CD8 V1
CCR5+/Dengue V1
CD69+/MAIT V1
Ki67+/EMRA CD4 V3
CD103+/CD8 V3
ICOS+ PD-1+/CD4 V3
CD69+/NK V3
CD27+/Dengue V3
Ki67+/CD56bri CD16dim V3
CD69+/CD8 V3
CD38+/Vd1 V3
CD45RA+/Dengue V3
LIF V3
MIG V3
CD38+/Vd2 V3
CD38+ CCR7-/MAIT V3
CD45RO+/Dengue V3
IL-1 beta V3